https://dx.doi.org/10.1016/j.conbuildmat.2019.117251

Durability Assessment of Reinforced Concrete Structures Considering Global Warming: A Performance-Based Engineering and Experimental Approach

Hongyuan Guo[1,2,3], You Dong[3,*], and Xianglin Gu[1,2]

1. Key Laboratory of Performance Evolution and Control for Engineering Structures of Ministry of Education, Tongji University, 1239 Siping Rd., Shanghai 200092, China
2. Department of Structural Engineering, College of Civil Engineering, Tongji University, 1239 Siping Rd., Shanghai 200092, China
3. Department of Civil and Environmental Engineering, Hong Kong Polytechnic University, Hong Kong 999077, China

Abstract: Reinforced concrete (RC) structures under marine atmospheric environment usually suffer from chloride ingress, which could impair structural serviceability and performance within the service life. Performance-based engineering, as an approach to design structures with predictable and defined performance, has attracted increased attention. In this paper, the developed probabilistic performance-based durability engineering (PBDE) approach is used as a novel attempt to integrate different computational modules (i.e., exposure analysis, deterioration, repair analysis, and impact/consequence analysis) within the durability assessment and management process of RC structures incorporating the experimental results. To begin with, a probabilistic environmental model is developed using the measured data to account for global warming, the seasonal and daily variation of temperature, etc. Additionally, deterioration analysis is conducted considering two-dimensional chloride transport and non-uniformity of corrosion. The experimental studies are conducted to verify the relevant numerical results. Subsequently, consequence analysis is performed to aid the maintenance process of RC structures. Uncertainties associated with material properties, model, and environmental scenarios, as well as the effect and cost of maintenance actions, are incorporated within the developed framework, which is illustrated using a real-world example. Compared to the traditional durability assessment approach, non-uniformity of corrosion, 2D convection-dominated chloride transport model, and climate change effects are assessed in a probabilistic manner.

Keywords: Durability; Performance-based engineering; Experimental study; Global warming; 2D chloride transport; Reinforced concrete structure.

** **Corresponding Author**
E-mail address: you.dong@polyu.edu.hk
Tel.: +852-3400 8818

1. Introduction

Nowadays, sustainable design and management of reinforced concrete (RC) structures in a life-cycle context have received increased interest within civil engineering. During the service life, the RC structures may be subjected to different deterioration scenarios, which could affect structural durability and long-term performance. The 2017 ASCE infrastructure report card showed that 56,007 bridges suffered from structural deficiency, and the estimated cost of rehabilitation was $123 billion in 2016 [1]. One of the significant issues associated with RC structures is the erosion media induced corrosion. A survey from the U.S. Government Accountability Office revealed that the cost caused by corrosion was $20.6 billion in 2016 [2]. The Chinese government spent approximately RMB 2.1 trillion, accounting for 3.34 % GDP in 2014 on the corrosion related issues [3]. Thus, the corrosion effect and its adverse influences on structural durability should be paid special attention to, and it is of great importance to establish a comprehensive framework to assess the durability of RC structures.

Under the marine atmospheric environment, RC structures suffer from chloride ingress [4]. Such physical phenomenon significantly affects the life-cycle design and maintenance philosophy. Studies have been conducted on different aspects of chloride ingression, such as the physical mechanism of chloride-induced deterioration [5–13] and durability design method [14–16]. However, due to the complexity of chloride-induced deterioration mechanism and lack of compatible and feasible physical models, a comprehensive and systematic durability framework for life-cycle assessment and decision making of RC structures is still missing by considering different aspects in a unified manner and more experimental studies should be conducted to verify the numerical results. Due to stochastic properties of the atmospheric environment and the unsaturated condition of concrete, the chloride transport in concrete is not only dominated by diffusion mechanism but also by convection mechanism [17,18]. In other words, a Fick-law based chloride transport model may misestimate the chloride profiles within the concrete and may be unsuitable for prediction of corrosion initiation. In this paper, the convection of chloride transport is observed within the experimental study and simulated by numerical modeling. Additionally, non-uniform corrosion and the two-dimensional (2D) chloride transport model should also be considered within the durability analysis. In this paper, the relevant aspects are considered, and experimental studies are conducted to verify the scenarios (e.g., convection mechanism, 2D transport).

Most traditional durability design philosophies are established based on deterministic or semi-probabilistic approach, such as Eurocode 2 [19], DuraCrete [20] and Standard for durability assessment of concrete structures (CECS) [21]. Under the traditional frameworks, the random properties of the varying climate and structural durability might not be well considered in life-cycle design and maintenance process. Additionally, the financial and social impacts were not well incorporated. Flint *et al*. [22] developed a performance-based durability engineering (PBDE) framework to evaluate the durability of RC structures considering the uncertainties and relevant costs. Concerning Flint's study [22], the application of PBDE is tentative and based on a simple case so that many related issues remained unsolved. For instance, a simplified 1D chloride transport model was adopted to evaluate corrosion initiation time without verifying its feasibility and accuracy. In this paper, the deterioration model is verified using in-situ environmental data and chloride ion measurement. Additionally, uncertainties associated with material properties, model, and environmental scenarios, as well as the effect and cost of maintenance actions, are incorporated within the developed framework, which is illustrated using a real-world example.

Existing studies revealed that the changing climate (e.g., temperature, relative humidity) might affect the durability of RC structures [23–26]. With the consideration of global warming, Bastidas-Arteaga *et al*. [24] indicated that the service life of the RC structures under the marine environment could be reduced by 2% to 18%. Also, the global warming could accelerate the chloride ingress and then increase corrosion rate [27], where Stewart *et al*. [27] found that corrosion rate may increase by 15% given 2 °C increase of temperature. Thus, it is of great importance to involve the changing climate, especially global warming, into the durability design and maintenance of RC structures. Though there exist some studies on the investigation of changing climate on structural durability, the relevant adverse effects on the durability-informed long-term financial and social impacts have not been addressed by previous studies. In this paper, considering the complexity and uncertainty in climate modeling, a rational and stochastic climate model within probabilistic PBDE framework is developed. Overall, a comprehensive probabilistic PBDE framework is proposed for the RC structures under the marine atmospheric environment considering global warming. To begin with, the proposed PBDE framework is introduced in Section 2. Then, in Section 3, the deterioration analysis model is established and verified by experimental data. A decision tree model is proposed to determine the repair strategies, and impact analysis is discussed in section 4. In Section 5, the proposed PBDE approach is applied to a real-world example by incorporating the in situ-experiment measurements. Finally, conclusions are drawn, and further work is noted.

2. Performance-based durability engineering (PBDE)

2.1. General framework

The integration of PBE framework within durability assessment was initially developed by Flint et al. [22]. In this study, the experimental studies were conducted to verify the adopted chloride penetration model and non-uniform deterioration. Subsequently, the relevant effects on the decision variables are quantified. This study could aid the application of the PBDE within structural durability-informed design and management process by incorporating experimental information to reduce the uncertainty within the PBE. As indicated in Fig. 1, the computational process can be divided into four stages: exposure analysis, deterioration analysis, repair analysis, and impact analysis. The outputs of these stages are exposure conditions (*EC*), damage measures (*DM*), repair action timing (t_{RA}), and decision information (*DI*). Uncertainty in each stage can be quantified by complementary cumulative distribution function (CCDF) (i.e., the probability of exceeding the value of the pinch-point variable). Due to the relation between adjacent stages, the CCDF of each analysis stage depends on the given pinch-point values from the prior stage in terms of conditional CCDF. The CCDF could be computed analytically or simulated by sampling methods. Once the probabilistic information of the computational stage is obtained, the CCDF of final decision information $G_{DI}(di)$ can be obtained as follows [22]

$$G_{DI}(di) = \iint G_{DI|t_{RA}}(di \mid t_{RA}) \mid dG_{t_{RA}|EC}(t_{RA} \mid ec) \mid\mid dG_{EC}(ec) \mid \quad (1)$$

where G_{EC} is the CCDF of the exposure condition; $G_{tRA|EC}$ is the conditional CCDF of repair combination under the given exposure conditions, and $G_{DI|tRA}$ is the conditional CCDF of decision information under the given repair combination. The final decision information of $\mathrm{G_{DI}}$ could be updated easily through changing the G_{EC}, $G_{tRA|EC}$, and $G_{DI|tRA}$ in Eq. (1).

2.2.Computational process of PBDE

As indicated in Fig. 1, an appropriate deterioration model should be established first. In this paper, the deterioration model considering chloride transport is established and verified using the experimental data. After the verification, the geometrical information, material properties, climate model, repair actions, and related impact information are assessed. To begin with, the exposure information *EC* (e.g., temperature, humidity, and surface chloride content) is identified. Within the step 2, the damage measures (*DM*) (e.g., the chloride content on the reinforcement surface C_{Cl}, the corrosion current density i_{corr}) are analyzed. The repair analysis is conducted in step 3, supposing that periodical inspection is executed. The repair actions are determined based on the inspection results. Also, the results of deterioration and repair action analyses are used for the next round of analysis. The loop would last until the end of service life, and probability mass function of repair combinations can be acquired, as shown in Fig.1. Finally, considering the probabilistic performance indices (e.g., cost and downtime) under given repair action, the decision information (*DI*) is obtained by Eq. (1). Uncertainties associated with material properties, model, and environmental scenarios, as well as the effect and cost of decision actions, are incorporated within the developed framework.

3. Exposure and deterioration analysis by numerical and experimental studies

As illustrated in Fig. 2, the deterioration analysis is a computational modulus embedded in the loop of the PBDE framework and is associated with several probabilistic parameters, e.g., heat transfer, moisture transfer, chloride content, corrosion rate, radius reduction, delamination. To accurately predict the corrosion initiation period, the 2D transport and convection of chloride ion are considered in this paper. Additionally, the experimental studies are conducted to verify the numerical results. Once the chloride content on the reinforcement surface reaches a critical value, the corrosion happens, and then the corrosion rate is assessed. The non-uniform corrosion is considered in this paper. The minimum reinforcement radius is adopted to calculate the cross-sectional loss and predict the delamination or concrete crack.

3.1. Environmental model

Within the PBDE framework, the environmental model is not only used for exposure analysis but also the identification of boundary condition in deterioration analysis. In exposure analysis, the environmental parameters are assessed in terms of characteristic values of *EC* (i.e., *ec*) and their probability distribution. The time-dependent environmental parameters, *ENV*(*ec*, *t*), Eq. (2) (e.g., temperature, relative humidity, and chloride content), consist of four parts: seasonal variation $ENV_{sea}(t)$, Eq. (3), daily variation $ENV_{daily}(t)$, Eq. (4), the increasing tendency ENV_{incre}(ec, *t*), Eq. (5), and zero-mean noise of environmental value λ.

$$ENV(ec,t) = ENV_{sea}(t) + ENV_{daily}(t) + ENV_{incre}(ec,t) + \lambda \tag{2}$$

$$ENV_{sea}(t) = a_1 \cdot sin\left[w_1 \cdot \left(t - t_{ref}\right)/365 + b_1\right] + a_2 \cdot sin\left[2 \cdot w_1 \cdot \left(t - t_{ref}\right)/365 + b_2\right] + bam \tag{3}$$

$$ENV_{daily}(t) = a_{01} - a_{11} cos(w_{11} \cdot t) + b_{11} sin(w_{11} \cdot t) - a_{21} \cdot cos(2w_{11} \cdot t) - b_{21} sin(2w_{11} \cdot t) \tag{4}$$

$$ENV_{incre}\left(ec,t\right) = a\left(ec\right)\cdot\left[\left(t-t_{ref}\right)/365\right]^{n(ec)} \tag{5}$$

where t is the time (day); t_{ref} is the reference time (day); bam is the baseline average mean annual value; a_1, a_2, b_1, b_2, w_1 and w_2 are the parameters of seasonal variation; a_{01}, a_{11}, a_{21}, b_{11}, b_{21} and w_{11} are the parameters of daily variation; and $a(ec)$ and $n(ec)$ are the parameters of the increasing tendency of environmental parameters based on the characteristic exposure condition. To account for the global warming effects, the temperature rising is predicted by a power function Eq. (5) and parameters $a(ec)$ and $n(ec)$ are acquired by fitting the measured data [22].

3.2. Corrosion initiation stage

3.2.1. Chloride transport model

Considering the binding capacity of cement, the total content of chloride C_{tc} contains two parts: bound chloride content C_{bc} (kg/m^3 of concrete) and free chloride content C_{fc} (kg/m^3 of pore solution).

$$C_{tc} = C_{bc} + w_e C_{fc} \tag{6}$$

where w_{e} is evaporable water content (m^3 pore solution/m^3 concrete). Existing study showed that ignoring convection mechanism of chloride transport may misestimate the corrosion initiation time and its uncertainty [23]. Thus, this paper employs a diffusion-convection model of chloride transport as [28]

$$\frac{\partial C_{fc}}{\partial t} = D_c^*\left(\frac{\partial^2 C_{fc}}{\partial x^2}+\frac{\partial^2 C_{fc}}{\partial y^2}\right) + D_h^*\left(\frac{\partial}{\partial x}\left(C_{fc}\frac{\partial h}{\partial x}\right)+\frac{\partial}{\partial y}\left(C_{fc}\frac{\partial h}{\partial y}\right)\right) \tag{7}$$

where x and y denote the horizontal and vertical coordinates (m) in cross-section; h is the relative humidity (RH) in pore solution; and D_{c}^* and D_{h}^* denote the apparent diffusion coefficients of chloride and humidity, respectively.

$$D_c^* = \frac{D_{c,ref}\, f_{c1}(T)\, f_{c2}(t)\, f_{c3}(h)}{1+\left(1/w_e\right)\left(\partial C_{bc}/\partial C_{fc}\right)},\quad D_h^* = \frac{D_{h,ref}\, f_{h1}(T)\, f_{h2}(t)\, f_{h3}(h)}{1+\left(1/w_e\right)\left(\partial C_{bc}/\partial C_{fc}\right)} \tag{8}$$

where $D_{c,ref}$ and $D_{h,ref}$ are the reference diffusion coefficients of chloride and humidity, respectively [29] and $\partial C_{bc}/\partial C_{fc}$ denotes the binding capacity of cement. Due to the failure of Freundlich isotherm in low C_{fc} [30], Langmuir isotherm [31] is employed herein

$$C_{bc} = \frac{\alpha_L C_{fc}}{1+\beta_L C_{fc}}, \tag{9}$$

in which α_L and β_L are binding constants; $f_{c1}(T)$, $f_{c2}(t)$, and $f_{c3}(h)$ are the influencing factors of temperature (K), time (d), and relative humidity on chloride transport; and $f_{h1}(T)$, $f_{h2}(t)$, and $f_{h3}(h)$ are the influencing factors of temperature, time, and relative humidity on moisture transport, respectively.

$$f_{c_1}(T) = \exp\left[\frac{U_c}{R_{gas}}\left(\frac{1}{T_{ref}}-\frac{1}{T}\right)\right],\ f_{c_2}(t) = \left(\frac{t_{ref}}{t}\right)^m,\ f_{c_3}(h) = \left[1-\frac{(1-h)^4}{(1-h_c)^4}\right]^{-1} \tag{10}$$

$$f_{h_1}(T) = \exp\left[\frac{U_h}{R_{gas}}\left(\frac{1}{T_{ref}}-\frac{1}{T}\right)\right],\ f_{h_2}(t_e) = 0.3+\sqrt{\frac{13}{t_e}},\ f_{c_3}(h) = \alpha_0 + \frac{1-\alpha_0}{1+\left((1-h)/(1-h_c)\right)^n} \tag{11}$$

where U_c and U_h denote the activation energy of the chloride diffusion and moisture diffusion respectively; R_{gas} is the gas constant; T and T_{ref} are the current and reference temperature (K), respectively; t, t_{ref}, and t_{e} are the current, reference and equivalent hydration time (d) respectively; h_c is reference relative humidity (RH) in pore solution; and α_0 is a parameter representing the ratio of $D_{h,\,min}$ to $D_{h,\,max}$.

For the description of moisture ingression, most of the previous studies focused on the diffusion mechanism [29,30,32–34]. Herein, the relative humidity h and moisture diffusion is used to describe moisture transport [28].

$$\frac{\partial w_e}{\partial h}\frac{\partial h}{\partial t} = div(D_h grad(h)) \tag{12}$$

where D_h is the humidity diffusion coefficient (m^2/s). In 1972, Bažant *et al.* [35] proposed a nonlinear empirical model of humidity diffusion coefficient D_h

$$D_h(h) = D_{h,ref}\left(\alpha_0 + \frac{1-\alpha_0}{1+\left((1-h)/(1-h_c)\right)^n}\right) \tag{13}$$

where $D_{h,ref}$ is the reference D_h and α_0 is the ratio of $D_{h,min}$ to $D_{h,max}$ (ranging between 0.025 and 0.10); and h_c is the reference humidity. Furthermore, Saetta *et al*. considered the influences of temperature T (K) and hydration time t_e (day) and suggested a model for humidity diffusion coefficient [36]

$$\begin{aligned}
&D_h(T,t,h) = D_{h,ref}\, f_{h1}(T)\, f_{h2}(t)\, f_{h3}(h),\\
&f_{h_1}(T) = \exp\left[\frac{U_h}{R}\left(\frac{1}{T_{ref}} - \frac{1}{T}\right)\right],\\
&f_{h_2}(t_e) = 0.3 + \sqrt{\frac{13}{t_e}},\\
&f_{c_3}(h) = \alpha_0 + \frac{1-\alpha_0}{1+\left((1-h)/(1-h_c)\right)^n}
\end{aligned} \tag{14}$$

where U_h denotes the activation energy of the moisture diffusion. Based on absorption theory, Brunauer *et al*. [36] proposed a three-parameter Brunauer-Skalny-Border isotherm (BSB model) to predict the moisture content w_e. Then, based on the BSB model, Xi *et al.* [37] established a three-parameter model of the adsorption isotherm

$$\begin{aligned}
&w_e = \frac{Ck_sV_mh}{(1-k_sh)\left[1+(C-1)k_sh\right]},\\
&C = \exp(855/T), k_s = \frac{\left[1-(1/N)\right]C-1}{C-1},\\
&N = (2.5+15/t)(0.33+2.2w/c)N_{ct},\\
&V_m = (0.068-0.22/t)(0.85+0.45w/c)V_{ct},
\end{aligned} \tag{15}$$

where V_{ct} and N_{ct} are the factors relating to cement type. Being different from the absorption process or wetting process, desorption process or drying process often presents a lagged phenomenon viz. Hysteresis Effect [38,39]. Although scholars have proposed drying and wetting curves based on the micro properties of concrete [38–40], it may be complicated for practical application. Lin *et al*. [41] developed a simplified way of changing the moisture diffusivity coefficient during drying and wetting periods. Lin's approach focused on the ideal wetting process and drying process, while the scanning process seems to be more common than the ideal wetting process and drying process in practical engineering. Besides, according to the relative humidity response test of OPC, Min *et al*. found that the coefficient of moisture diffusion is about 3×10^{-10} m^2/s under the drying process and 15×10^{-10} m^2/s under the wetting process [42]. In this paper, given the expression of absorption isotherm Eq. (15), the $D_{h,ref}$ in Eq. (14) is replaced by $D^{dry}{}_{h,ref}$ when h decreases; and the $D_{h,ref}$ in Eq. (14) is replaced by $D^{wet}{}_{h,ref}$ when h increases.

For the heat transfer process, a differential equation proposed by Bastidas-Arteaga [24] is employed

$$\rho_c c_q \frac{\partial T}{\partial t} = \lambda\left(\frac{\partial^2 T}{\partial x^2} + \frac{\partial^2 T}{\partial y^2}\right) \tag{16}$$

where T is the current temperature (K) and ρ_c, c_q and λ denote the density, heat capacity, and thermal conductivity of concrete, respectively.

The calculation process of chloride ingression is divided into three steps: solving the heat transfer equation (Eq. (16)), solving moisture transfer equation (Eq. (12)) based on the solution of the heat transfer equation, and finally solving the chloride transfer equation (Eq.

(7)). All boundary conditions are obtained through the environmental model (i.e., Eqs.(2)-(5)). Eqs. (12) and (7) are associated with high nonlinearity. The alternating-direction implicit (ADI) finite-difference method developed by Peaceman and Rachford is used to solve the partial differential equations.

3.2.2. Verification of chloride transport model by experimental studies

In this study, the chloride transport model is verified using experimental data. The process of verifying the chloride transport model can be divided into three steps: (1) Build an in-situ experimental field and prepare concrete specimen; (2) Monitor and record the environmental information and chloride profiles inside concrete specimen; and (3) Compare the experimental results with numerical simulation. As shown in Fig. 3, the experimental field is located in the coastal area. The real-time local relative humidity (RH) and temperature are measured. The cubic specimens of ordinary concrete with the dimensions of 150 × 150 × 150 mm or 100 × 100 × 100 mm are cast and cured for 28 days. After curing, the surfaces of concrete cubic are sealed by epoxy resin to achieve 1D or 2D chloride transport. Next, the specimens are transferred for the exposure test.

The following step is to capture the chloride profiles, which could be used to compare with numerical results and testify the feasibility of the numerical model. The chloride profiles of concrete need to be destructively tested regularly. The experimental interval varies from six months to 1 year. The concrete cubic is taken for the chloride content test. As shown in Fig. 4, given a profile interval, e.g., 3 mm or 5 mm, the power samples at different depths of the specimen are collected through a bench drilling machine and dissolved in a bottle of acid extract liquor for 24 hours. Next, the chloride concentration in the acid extract liquor is measured by the direct potentiometry with the help of electrode and measurement device. The recorded potentiometry in the bottles is converted into the chloride concentration at different depths, which could be used to draw the scatter plot of chloride content versus ingress depth.

3.3.Propagation stage

Once the chloride content on concrete cover exceeds critical chloride content C_{cr} (wt % of cement, a gauss random variable with a mean value of 0.4% and a standard deviation (STD) of 0.1% [16,22]), reinforcement corrosion occurs [8]. Considering the influences of chloride content, temperature and time on corrosion rate $i_{\mathrm{corr}}(t)$ (uA/cm^2), an empirical model of corrosion rate developed by Liu is used [9]

$$\begin{aligned} \ln(1.08 i_{corr}(t)) = 7.89 + 0.7771\ln(1.69Cl) - 3006/T \\ -0.000116R_c + 2.24t^{-0.215} + N(0, 0.3312) \end{aligned} \tag{17}$$

where Cl denotes chloride content (kg/m^3); $T(K)$ is the temperature at the concrete inside; R_{c} (Ohms) is the resistance of cover concrete (e.g., 25000 Ohms [22]); t (year) is the time since corrosion initiation; and $N(0, 0.3312)$ is the aleatory component of corrosion rate. According to Faraday law, the average reinforcement diameter loss $\Delta r\ (t)$ can be computed by Eq. (18) [43]

$$\Delta r(t) = \int 0.0116 i_{corr}(t) dt \tag{18}$$

Given the circular cross-section, the average corrosion ratio of steel bar can be calculated

$$\eta_s(t) = 1 - \left[r_0 - \Delta r(t)\right]^2 / r_0^2 \tag{19}$$

In general, due to the complex chloride transport mechanism and non-uniformity of material properties, chloride ingress may induce macro-cell corrosion of reinforcement (e.g., pitting corrosion or localized corrosion). Most of existing studies used the pitting factor to quantify the pitting corrosion based on the assumption of one-single pit [44, 45]. However, in practical engineering, the cross-section of corroded rebar might be complex due to distribution of different numbers of corrosion pits. Thus, it is difficult to assess the pattern of pitting corrosion by using pitting factor and minimum rebar diameter. Then, Zhang et al. [46] and Gu et al. [12] proposed the *R* factor of non-uniform corrosion to quantify the corrosion geometry for both uniform corrosion and pitting corrosion based on both experimental and numerical studies. *R* factor is the ratio of the average cross-sectional area to the minimum cross-sectional area. Gu *et al.* [12] conducted the salt-spray test of RC slabs to obtain corroded steel bars, then used 3D scanner to acquire the distribution of cross-sectional area. According to statistics analysis, *R* values of corroded steel bar were collected, and the *R* factor was found to follow Type I extreme distribution (Gumbel distribution). The distribution parameters μ_0 (Eq. (20)) and σ_0 (Eq. (21)) of *R* factor are obtained from the statistics result of cross-sectional areas of rebar [12].

$$\mu_0(t) = 3.35\eta_s(t)\mathrm{e}^{-0.236 i_{corr}(t)} + 0.12\eta_s(t) + 1.01 \tag{20}$$

$$\sigma_0(t) = 0.3371\eta_s(t) + 0.0006 \tag{21}$$

$$A_0 = \pi D_0 L_0 \tag{22}$$

where D_0 is the initial diameter of rebar; L_0 is the analysis length and A_0 is rebar surface area. According to the theory of extreme value, Eq. (23) is employed to calculate the distribution parameters of the *R* factor under the surface area *A*

$$\mu(t) = \mu_0(t) + \sigma_0(t)\ln(A/A_0), \sigma(t) = \sigma_0(t) \tag{23}$$

The R factor is related with the corrosion current density and corrosion degree, but R factor refers to cross-sectional area, rather than the steel bar radius or diameter. Herein, the cracking of concrete cover happens once the equivalent maximum radius loss Δr_{max} (i.e., r_0 - r_{min}) exceeds Δr_{cr}. In this paper, an equivalent maximum radius loss Δr_{max} is proposed to quantify the corrosion level and testify whether the cover crack happens or not. The detailed investigation on the pitting corrosion (e.g., number of pits within a given section, geometry of steel bar after corrosion) is beyond the scope of this study. In this paper, the r_{min} is approximately computed by an equivalent r_{min} as follows

$$r_{\min}(t) = \frac{r_0 - \Delta r(t)}{\sqrt{R(t)}} \tag{24}$$

4. Repair and impact analysis

The purposes of repair and impact analysis are to provide the application timing of different repair actions. Supposing that regular inspection and special inspection are executed every two and ten years, respectively, three repair technologies are provided: Cathodic protection (*CP*) ra_1, cathodic prevention (*CPre*) ra_2, and patch repair ra_3 [22]. According to the design reference period (50 years) in GB50068-20001 [47], the validity period of CP and CPre are assumed as 15 and 17 years, respectively. Meanwhile, two types of decision information (i.e., cost and downtime associated with the repair actions) are considered. As there are limited information on the maintenance cost and downtime associated with different maintenance actions in China, the relevant parameters used are based on the previous studies. Given more validated information, the values of these parameters could be easily updated. Assuming the decision information follows Gaussian distribution ($N(\mu^*, \sigma^*)$, μ^* denotes the mean and σ^* denotes the standard deviation), the initial costs (USD) of CP, CPre and Patch repair are $N(250, 80)$, $N(150,40)$ and $N(100,20)$ and their downtimes (months) are $N(24,6)$, $N(6,2)$ and $N(4,1)$, respectively. During the service period of CP and CPre, both of their ongoing cost (USD/year) are $N(5,1)$.

As illustrated in Fig. 5, a decision tree model is adopted to determine the types and timing of repair actions. Repair actions are supposed to be activated when delamination occurs under regular inspection or special inspection. *CP* would be applied for the first time of repair, where the concrete cover is replaced, and the chloride ion is cleared. After the validity period of *CP*, *CPre* is used to prevent corrosion initiation. If the residual life is larger than 10 years, but less than 20 years, *patch repair* is utilized to clear the chloride on the concrete surface. Supposing the random variables of cost and downtime associated with each maintenance action are independent, the mean ($\mu_{\mathrm{rc\_cost}}$ and $\mu_{\mathrm{rc\_downt}}$) and STD ($\sigma_{\mathrm{rc\_cost}}$ and $\sigma_{\mathrm{rc\_downt}}$) of a given repair combination are computed by summing all mean values of variables and taking the square root of the sum of squares, as follows

$$\begin{aligned}
\mu_{\mathrm{rc_cost}} &= 250 \cdot H(t_{ra_1}) + 5t_{ra_1} + 150 \cdot H(t_{ra_2}) + 5t_{ra_2} + 100 \cdot H(t_{ra_3}) \\
\mu_{\mathrm{rc_downt}} &= 24 \cdot H(t_{ra_1}) + 6 \cdot H(t_{ra_2}) + 4 \cdot H(t_{ra_3}) \\
\sigma_{\mathrm{rc_cost}} &= \sqrt{\left[80 \cdot H(t_{ra_1})\right]^2 + t_{ra_1}^2 + \left[40 \cdot H(t_{ra_2})\right]^2 + t_{ra_2}^2 + \left[20 \cdot H(t_{ra_3})\right]^2} \\
\sigma_{\mathrm{rc_downt}} &= \sqrt{\left[6 \cdot H(t_{ra_1})\right]^2 + \left[2 \cdot H(t_{ra_2})\right]^2 + \left[H(t_{ra_3})\right]^2}
\end{aligned} \tag{25}$$

where $H(\cdot)$ denotes the Heaviside function ($H(x) = 1$ when $x > 0$; $H(x) = 0$ when $x <= 0$) and t_{ra1}, t_{ra2} and t_{ra3} are the durations (months) of *CP*, *CPre*, and Patch repair, respectively. Finally, given the probability distribution of repair combination, the final decision information can be easily obtained through the convolution method, viz. Eq. (1).

5. Illustrative example

As illustrated in Fig. 6, an RC beam with the ordinary Portland cement of 0.53 water-to-cement ratio, a cross-section of 200 × 400 mm and a cover thickness of 25 mm, located on the west coast of Yellow Sea, is investigated to demonstrate the feasibility and applicability of the proposed PBDE framework. The reinforcement layout of this beam is 3ϕ25, and analysis length for R factor is determined as 150 mm [44]. The beam was built in 2010. Eight cases are assessed under different scenarios, as shown in Table 1. The relevant calculation parameters and values in Eqs. (6)-(16) are listed in Table 2.

To conduct the exposure analysis, characteristic exposure condition (ec) of temperature is assumed as a random variable following $0.5N(1.80,0.2) + 0.5N(3.00,0.13)$ and λ is the zero-mean noise component with 0.475 °C STD [22]. Considering global warming, the parameters $a(ec)$ and $n(ec)$ in the increasing tendency Eq. (5) of temperature are calculated through Eqs. (26) and (27) [22].

$$a(ec) = 5.04\times10^{-3}ec^2 - 3.57\times10^{-2}ec + 6.49\times10^{-2} \tag{26}$$

$$n(ec) = 3.59\times10^{-1}ec + 3.33\times10^{-1} \tag{27}$$

In this paper, the environmental information is based on the measurement data of the west coast of the Yellow Sea from 2011 to 2012 by using temperature and humidity sensor, DB 170 (Dalian Beifang M&C Engineering Co., Ltd., China) with the accuracy of ±1.8% for RH and ±0.3 °C under 25 °C [17]. Then, by curve-fitting, the parameters used in Eqs. (2)-(5), (26) and (27) are obtained as listed in Table 3. Fig. 7 illustrates the comparisons of fitting surrounding temperature and relative humidity versus measured data.

5.1.Model verification

5.1.1. Influences of convection on chloride transport

A calculation case was supplied to compare the chloride profiles within concrete. Supposing that the boundary condition is the constant content of free chloride ion (wt % of cement) 0.5 % and other environmental parameters remain unchanged, the chloride profiles of three instants (2 years, 10 years, and 20 years) under with and without convection assumption are obtained respectively. As shown in Fig. 8, all three curves with convection assumption are about 100 ~ 136% times those without convection. Also, the curves with convection appear non-linearity i.e., one peak at the depth of 3 mm. On the other hand, in Fig. 8, the highest chloride content appears in the 2-th year, but the deepest chloride transport was shown in the 20-th year. Due to the various surrounding environments, the influences of convection on the chloride transport and durability assessment may be hard to evaluate precisely, but the effects of convection on structural durability and performance is negative. Thus, it is necessary to consider the convection effect in the performance based-durability assessment.

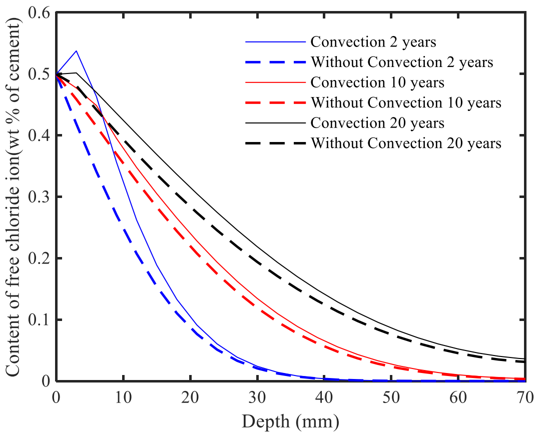

Fig. 8. Comparison of free chloride profiles within concrete under the assumptions of with

and without convection

5.1.2. *Comparison between model prediction and experimental data*

The filed experimental data of chloride ingress in the concrete specimen are collected to verify the accuracy of the adopted chloride transport model [17]. The concrete blocks were taken out regularly to drill the powder and measure the chloride concentration. The chloride profiles after 6, 22, and 34 months are shown in Fig. 9. As indicated, the numerical curves after 6 and 22 months are relatively higher than experimental curves, but after 34 months, the numerical curve is surpassed by experimental one. As illustrated in Fig. 9, the convolution zone does not appear in the profiles of chloride content until 34 months. The depth of the actual convolution zone after 34 months is about 13.5 mm while the depth of the simulated convolution zone after 34 months is about 10.5 mm in Fig.9a. The difference may arise from several reasons: (1) Lack of precise surface chloride and (2) Lack of other environmental factors, e.g., wind load, rain, snow, etc. On the other hand, due to the absence of convection mechanism, the depth of the simulated convolution zone after 34 months is about 7.5 mm in Fig.9b which is smaller than Fig. 9a.

5.2.PBDE framework

5.2.1. *Exposure and deterioration analysis*

Fig. 10 shows the continuous curve and scatter points of CCDF of exposure condition, where scatter points denote the characteristic exposure condition ec_1, $ec_2 \ldots ec_{10}$. Next, given ec_1, $ec_2, \ldots, ec_{10}$, samples of C_{cr}, Δr_{cr}, and R factor are generated by Sobol quasi-random sequence.

Fig.11 presents the PDF contour of chloride content on the surface of the steel bars for cases 1 and 5. Without repair actions, the contour bands in Fig.10a and c are fluctuating and continuous reflecting the variation of environmental parameters. Considering the repair actions, the contour bonds in Fig.11b and d are dispersedly distributed. The mean values in Fig.11b and d show a fluctuation, which is more apparent than Fig.11a and c. Thus, the proposed chloride transport model can reflect the effects of changing climate on chloride transport. By using the 2D chloride transport model and without repair, the mean value of chloride content on the surface of the corner steel bars is about 1.29 ~ 4.49 times of the middle steel bars.

The mean and STD of chloride content on the steel bar surface of Cases 1, 3, 5, and 7 are presented in Fig. 12. The curves in Fig.12 show a strong and periodic fluctuation. As shown in Fig. 12, the mean and STD of 'Case 1 corner bar' are close to 'Case 5 corner bar' from 2010 to 2018, but then the mean values of 'Case 5 corner bar' become much more fluctuating but 10 % ~ 46 % lower than 'Case 1 corner bar'. Thus, applying repair actions could effectively reduce the mean value of chloride content on the steel bar surface.

Fig. 13 shows the mean and STD i_{corr} of steel bar in Cases 1, 3, 5, and 7. As indicated, during most of the investigated time interval, mean and STD i_{corr} of the corner steel bars are less than 0.10 μA/cm^2 and 0.15 μA/cm^2, and only a few ones exceed 0.16 μA/cm^2 and 0.21 μA/cm^2. Due to the application of repair actions on time, the mean i_{corr} of the middle steel bars is much smaller than that of the corner steel bars. The maximum means of i_{corr} of 'Case 1 corner bar' and 'Case 5 corner bar' are 0.1525 μA/cm^2 and 0.0848 μA/cm^2, which are twice of the maximum i_{corr} of 'Case 3 corner & middle bar' 0.815 μA/cm^2 and 'Case 7 corner & middle bar' 0.0411 μA/cm^2, respectively. The maximum mean i_{corr} of 2D chloride transport is about twice the maximum i_{corr} of 1D chloride transport.

Furthermore, Fig.14 and Fig.15 show the mean and STD of the average loss of reinforcement radius Δr and maximum loss of reinforcement radius Δr_{max} of Cases 1 ~ 8, respectively. As indicated in Figs.14a, without repair action, the mean Δr of 'Case 1 corner bar' is at least 1.447 times higher than the Δr associated with Case 3; and the mean Δr of 'Case 1 middle bar' is about 0.882 ~ 1.381 times of the Δr of Case 3. Besides, Fig.14c shows that the STD Δr of 'Case 1 corner bar' is higher than that of Case 3 before 2049 but surpassed by Case 1 after 2049; and the STD of Δr of 'Case 1 middle bar' is about 0.966 ~ 1.358 times of the Δr associated with Case 3. In Fig.14b, the mean Δr of 'Case 5 corner bar' is at least 1.76 times of the mean Δr in Case 7. Besides, Fig.14d shows the STD of Δr of Case 5 and Case 7. Comparing Fig.14a with b, repair action could significantly reduce the mean Δr by about 85% for corner steel bar and about 99% for the middle steel bar under 2D transport. Meanwhile, the STD of Δr decreases by about 57% for corner steel bar and about 68% for the middle steel bar.

As indicated in Fig.15a, the ratio of the mean of maximum radius loss $\Delta r_{\max}$ under 'Case 1 corner bar' to 'Case 2 corner bar' varies from 1.239 to 5.162 and the ratio of the mean $\Delta r_{\max}$ under 'Case 1 middle bar' to 'Case 2 middle bar' varies from 2.236 to 4.823. In Fig.15c, the ratio of STD of $\Delta r_{\max}$ under 'Case 1 corner bar' to 'Case 2 corner bar' is larger than 5.308 and the ratio of STD of $\Delta r_{\max}$ under 'Case 1 middle bar' to 'Case 2 middle bar' is larger than 1.725. Thus, corrosion non-uniformity is a vital factor in deterioration.

Without repair action, the mean value of $\Delta r_{\max}$ associated with 'Case 1 corner bar' is at least 1.619 times larger than Case 3, and the ratio of the mean $\Delta r_{\max}$ under 'Case 1 middle bar' to Case 3 ranges from 0.886 to 1.702. Also, the STD of $\Delta r_{\max}$ of 'Case 1 corner bar' is at least 6.3109 times larger than Case 3, and the ratio of the STD of $\Delta r_{\max}$ under 'Case 1 middle bar' to Case 3 ranges from 0.986 to 1.047. Given repair actions, the relevant ratios could also be computed. Repair action could significantly reduce the mean of Δr_{max} by about 85% for corner steel bar and about 99% for middle steel bar under 2D chloride transport, meanwhile the STD of Δr_{max} decreases by about 56% for corner steel bar and about 69% for middle steel bar.

The influences of global warming within 50 years (ΔT_{50}) on the durability are assessed. Three additional cases of ΔT_{50} are applied: 0.3°C, 3°C, and 6°C. Eq. (5) is replaced by Eq. (28) to achieve a ΔT_{50} controlled temperature model.

$$ENV_{new,incre}\left(\Delta T,ec,t\right) = ENV_{incre}\left(ec,t\right)\cdot\frac{\Delta T}{E\left[env_{incre}(ec,50a)\right]-E\left[env_{incre}(ec,0a)\right]} \tag{28}$$

Figs. 16 – 18 illustrate the mean and STD of chloride concentration on the steel bar surface, corrosion current density, Δr and $\Delta r_{\max}$, respectively. In Fig. 16, the influences of ΔT_{50} on the STD of C_{Cl} (Figs. 16c and d) are slightly more than the mean of C_{Cl} (Figs. 16a and b) both on the middle bar and the corner bar. However, the effects of ΔT_{50} on the STD of i_{corr} (Figs. 17c and d) are more significant than the mean of i_{corr} (Figs. 17a and b). In Fig. 18, ΔT_{50} has an apparent effect on the evolution process of radius loss Δr and $\Delta r_{\max}$. Table 4 lists all ratios of the mean and STD of chloride content C_{Cl}, corrosion current density i_{corr}, radius loss Δr and $\Delta r_{\max}$ under different ΔT_{50} to Case 1 (only the values at 50a are selected to compare). As indicated, most C_{Cl}, i_{corr}, Δr and $\Delta r_{\max}$ are approximately linear to ΔT_{50} expect that the i_{corr} of the corner bar. The mean and STD of C_{Cl} increases by about 0.4 ~ 0. 6 % and 3 % given 1°C increase of ΔT_{50}, respectively; the STD of C_{Cl} increase by about 3 % given 1°C increase of ΔT_{50}; the mean and STD of i_{corr} on middle bar increase by about 21 % and 37% given 1°C increase of ΔT_{50}, respectively; the mean and STD of radius loss increases by about 2% given

1°C increase of ΔT_{50}.

5.2.2. Repair and impact analysis

Fig.19 compares the probability mass function (PMF) of the convoluted timing of repair actions under Cases 5 ~ 8. In Cases 5 and 6, 'CP2020 & CPre2036' (Combination 2) owns the highest probability of 0.4218 (Case 5) and 0.4472 (Case 6), followed by 'CP2030 & Patch2050' (Combination 5) with the probability of 0.2839 (Case 5) and 0.4306 (Case 6). The 'CP & CPre' (Combination 1 and 2) and 'CP & Patch' (Combination 3, 4, and 5) are the most common repair combinations. The probability of 'CP & CPre' is 0.4281 in Case 5 and 0.4472 in Case 6, and the probability of 'CP & Patch' is 0.4515 in Case 5 and 0.4306 in Case 6. Thus, non-uniform corrosion has few effects on the probability of the repair combinations but affects their timings. Fig.15 shows that Δr_{max} of Case 5 might be 4.4 times larger than Case 6 and concrete cracking happens in Case 5 but does not occur in Case 6. Thus, Case 5 can apply repair actions after regular and special inspection, but Case 6 applies repair action only after special inspection.

Also, from Cases 5 ~ 8, chloride transport has much more influences on the timing of repair combination than corrosion non-uniformity. As presented in Fig.19, considering 2D chloride transport, repair action happens during the service life. If only under 1D chloride transport, 'No repair' could result within the 50 years.

According to the PMF of convoluted timing and impact information of repair actions, the distribution of final lifetime decision is obtained by Eq. (25), as shown in Fig. 20. The curve shapes of Fig.20a and b are similar. $G_{DI1}(0)$ and $G_{DI2}(0)$ of Cases 7 and 8 equal 0.69 due to the existence of 'No Repair' in Cases 7 and 8, while $G_{DI1}(0)$ and $G_{DI2}(0)$ of Cases 5 and 6 equal 1.

Thus, the mode of chloride transport has a more significant effect on the CCDF of decision information than corrosion non-uniformity. Comparing Case 5 with Case 7, the mean values of cost μ_{cost} and downtime μ_{downtime} associated with Case 5 are 108.92% and 86.15% higher than that of Case 7. The STD of cost σ_{cost} and downtime σ_{downtime} of 2D chloride transport are about 25% and 36% lower than those of 1D chloride transport.

A parametric analysis is conducted to study the effect of the distribution parameters associated with the maintenance cost and downtime on the decision variable. Concerning the three types of repair actions in this paper, scaling factor x_i (i = 1,2, and 3) is supposed to update the distribution parameters (mean and STD) of ra_i by multiplying the x_i and original the distribution parameters of ra_i (viz. enlarge or reduce the distribution parameters of information parameters within one type of repair action). Then, the distribution parameters of decision information (μcost, μdowntime, σcost, and σdowntime) with updated distribution parameters of rai can be calculated. Besides, A response surface model (RSM) is applied as follows

$$\begin{aligned} y &= \beta_0 + \beta_1 x_1 + \beta_2 x_2 + \beta_3 x_3 \\ &\quad + \beta_4 x_1^2 + \beta_5 x_1 x_2 + \beta_6 x_1 x_3 + \beta_7 x_2^2 + \beta_8 x_2 x_3 + \beta_9 x_3^2 \end{aligned} \tag{29}$$

where β_k (k = 0, 1, …, 9) is the coefficient of RSM function. Taking Case 5 as one example, 128 random samples of x_i are generated to fit the surface model Eq. (29) and then fitted coefficients are summarized in Table 5. Fig. 21 illustrates the distribution parameters of decision information versus x_i. In Figs. 21a and b, it could be found that the mean value of ra1 affects the mean values of cost and downtime much more significantly than those of ra_2 and ra_3. In Figs. 21c and b, the STD of ra_2 influences the STD of cost and downtime mostly.

6. Conclusions

In this paper, a probabilistic PBDE framework for RC structures under marine atmospheric environment is proposed incorporating different computational modules. A comprehensive deterioration analysis model is developed to account for the 2D chloride transport and non-uniformity of corrosion. The experimental studies are conducted to verify the numeral analysis. The uncertainty associated with material properties, model, and environmental scenarios, as well as the effect and cost of decision actions, are incorporated within the developed framework. The following conclusions are drawn:

(1) Based on the experimental and numerical analysis, it is crucial to take the convection effect of chloride transport into consideration within the deterioration analysis process. Without considering the convection mechanism of chloride transport, the chloride profile within concrete would not perform high-nonlinearity and match the actual experimental data. Overall, it would underestimate the deterioration scenario of RC structures.

(2) Deterioration analysis reveals that the repair action and fluctuated environmental parameters can affect the deterioration process of RC beam. As indicated, the repair action could reduce nearly 50% mean values of chloride content on the steel bar surface and corrosion current density i_{corr}. Further, the mean values of average Δr and maximum radius loss Δr_{max} of reinforcement decrease by 85~99% with repair action, but the STD of Δr and Δr_{max} decrease by 56~69% with repair action.

(3) On the other hand, without repair action, corrosion non-uniformity mainly affects Δr_{max}. The 2D chloride transport could increase the mean chloride content on the steel bar surface,

the mean i_{corr}, mean Δr, and mean Δr_{max} significantly. With the consideration of repair action, corrosion non-uniformity could slightly affect the deterioration process, and 2D chloride transport can increase the deterioration conditions. The differences between 2D chloride transport and 1D chloride transport are mitigated by repair action, which demonstrates the importance of maintenance actions within the service life of RC structures. Additionally, a sensitivity analysis shows that 1°C increase during the 50 years could lead to about 2% increase on the mean and STD of radius loss.

(4) Repair analysis shows that repair action could be activated earlier if corrosion non-uniformity is considered. Also, 2D chloride transport makes corrosion detected earlier, and the possibility of repair is much higher than that using 1D chloride transport.

(5) Impact analysis indicates that the mode of chloride transport dominates the CCDF of decision information cost and downtime, while they are not much affected by corrosion non-uniformity. Considering both the 2D chloride transport and non-uniform corrosion, the mean and STD of cost are 0.34% and 0.04% lower than the case, which only considers 2D chloride transport. Apart from that, comparing with 1D transport, 2D chloride transport could increase the mean of cost and downtime by about 110 % and 86 %. According to the RSM analysis, the mean value of ra_1 affects the mean values of cost and downtime most significantly, while the STD of ra_2 influences the STD of cost and downtime mostly.

In summary, it is feasible to apply the developed PBDE framework to evaluate the durability of RC structures. The proposed approach could aid the durability-informed design and management of civil infrastructures.

Acknowledgment

This study has been supported by The Hong Kong Polytechnic University under Start-Up Fund number 1-ZE7Q, a grant from the National Natural Science Foundation of China (Grant No. 51808476), the Research Grant Council of Hong Kong (ECS project No. PolyU252161/18E), and the Research Grants Council of the Hong Kong Special Administrative Region, China (Project No. [T22/502/18]). The opinions and conclusions presented in this paper are those of the authors and do not necessarily reflect the views of the sponsoring organizations. The first author wants to sincerely thank his friend Chuenki Chan who offers her love and companion and contributes much to this work.

References:

[1] American Society of Civil Engineers, Infrastructure report card, ASCE News. 53 (2013) 1–36. doi:10.1017/CBO9781107415324.004.

[2] U.S. Senate, Report to the Committee on Armed MANAGEMENT DOD Should Take Additional Actions to Enhance Corrosion Prevention and Mitigation Efforts, (2018).

[3] H. Baorong, L. Dongzhu, Corrosion Cost and Preventive Strategies in China, Strateg. Policy Decis. Res. 6 (2018) 009 (in Chinese). doi:10.16418/j.issn.1000-3045.2018.06.008.

[4] S.L. Amey, D.A. Johnson, M.A. Miltenberger, H. Farzam, Predicting the service life of concrete marine structures: An environmental methodology, ACI Struct. J. 95 (1998) 205–214. doi:10.14359/540.

[5] Y.P. Xi, Z.P. Bažant, Modeling Chloride Penetration in Saturated Concrete, J. Mater. Civ. Eng. 11 (1999) 58–65. doi:10.1061/(ASCE)0899-1561(1999)11:1(58).

[6] P.A.M. Basheer, S. Nanukuttan, J. Kim, T.M. Chrisp, B. Suryanto, W.J. McCarter, Chloride ingress into marine exposed concrete: A comparison of empirical- and physically- based models, Cem. Concr. Compos. 72 (2016) 133–145. doi:10.1016/j.cemconcomp.2016.06.002.

[7] A.C. Appleton, a Costa, A.C. Appleton, Chloride penetration into concrete in marine environment -Part I: Main parameters affecting chloride penetration, Mater. Struct. Constr. 32 (1999) 252–259. doi:10.1007/BF02479627.

[8] B.B. Zhou, X.L. Gu, H.Y. Guo, W.P. Zhang, Q.H. Huang, Polarization behavior of activated reinforcing steel bars in concrete under chloride environments, Constr. Build. Mater. 164 (2018) 877–887. doi:10.1016/j.conbuildmat.2018.01.187.

[9] T. Liu, R.W. Weyers, Modeling the dynamic corrosion process in chloride contaminated concrete structures, Cem. Concr. Res. 28 (1998) 365–379. doi:10.1016/S0008-8846(98)00259-2.

[10] P. Zdenek, M. Bazant, Physical Model for Steel Corrosion in Concrete Sea Structures - Application, J. Struct. Div. 105 (1979) 1154–1166.

[11] K.A.T. Vu, M.G. Stewart, Structural reliability of concrete bridges including improved chloride-induced corrosion models, Struct. Saf. 22 (2000) 313–333. doi:10.1016/S0167-4730(00)00018-7.

[12] X.L. Gu, H.Y. Guo, B.B. Zhou, W.P. Zhang, C. Jiang, Corrosion non-uniformity of steel bars and reliability of corroded RC beams, Eng. Struct. 167 (2018) 188–202. doi:10.1016/j.engstruct.2018.04.020.

[13] A.A. Torres-Acosta, S. Navarro-Gutierrez, J. Terán-Guillén, J. Terán-Guillénb, J. Terán-Guillén, Residual flexure capacity of corroded reinforced concrete beams, Eng. Struct. 29 (2007) 1145–1152. doi:10.1016/j.engstruct.2006.07.018.

[14] O.E. Gjørv, Durability design of concrete structures in severe environments, CRC Press, 2014.

[15] M. Akiyama, D.M. Frangopol, M. Suzuki, Integration of the effects of airborne chlorides into reliability-based durability design of reinforced concrete structures in a

marine environment, Struct. Infrastruct. Eng. 8 (2012) 125–134. doi:10.1080/15732470903363313.
[16] E. Bastidas-Arteaga, F. Schoefs, M.G. Stewart, X. Wang, Influence of global warming on durability of corroding RC structures: A probabilistic approach, Eng. Struct. 51 (2013) 259–266. doi:10.1016/j.engstruct.2013.01.006.
[17] H.F. Zhang, W.P. Zhang, X.L. Gu, X.Y. Jin, N.G. Jin, Chloride penetration in concrete under marine atmospheric environment – analysis of the influencing factors, Struct. Infrastruct. Eng. 2479 (2016) 1–11. doi:10.1080/15732479.2015.1134588.
[18] H.W. Song, C.H. Lee, K.Y. Ann, Factors influencing chloride transport in concrete structures exposed to marine environments, Cem. Concr. Compos. 30 (2008) 113–121. doi:10.1016/j.cemconcomp.2007.09.005.
[19] DS/EN 1992-1-1, Eurocode 2 : Design of concrete structures – Part 1-1: General rules and rules for buildings, (1992).
[20] Duracrete, DuraCrete: Probabilistic Performance based Durability Design of Concrete Structures - Final Technical Report: General guidelines for durability design and redesign, Lyngby, 2000.
[21] CECS, Standard for durability assessment of concrete structures., Beijing China Archit. Build. Press. (2007).
[22] M.M. Flint, J.W. Baker, S.L. Billington, A modular framework for performance-based durability engineering: From exposure to impacts, Struct. Saf. 50 (2014) 78–93. doi:10.1016/j.strusafe.2014.03.003.
[23] E. Bastidas-Arteaga, A. Chateauneuf, M. Sánchez-Silva, P. Bressolette, F. Schoefs, A comprehensive probabilistic model of chloride ingress in unsaturated concrete, Eng. Struct. 33 (2011) 720–730. doi:10.1016/j.engstruct.2010.11.008.
[24] E. Bastidas-Arteaga, A. Chateauneuf, M. Sánchez-Silva, P. Bressolette, F. Schoefs, Influence of weather and global warming in chloride ingress into concrete: A stochastic approach, Struct. Saf. 32 (2010) 238–249. doi:10.1016/j.strusafe.2010.03.002.
[25] E. Bastidas-Arteaga, M.G. Stewart, Economic assessment of climate adaptation strategies for existing reinforced concrete structures subjected to chloride-induced corrosion, Struct. Infrastruct. Eng. 12 (2016) 432–449. doi:10.1080/15732479.2015.1020499.
[26] R.A. Medeiros-Junior, Impact of climate change on the service life of concrete structures, Elsevier Ltd, 2017. doi:10.1016/B978-0-08-102181-1.00003-4.
[27] M.G. Stewart, X. Wang, M.N. Nguyen, Climate change impact and risks of concrete infrastructure deterioration, Eng. Struct. 33 (2011) 1326–1337. doi:10.1016/j.engstruct.2011.01.010.
[28] D. V. Val, P.A. Trapper, Probabilistic evaluation of initiation time of chloride-induced corrosion, Reliab. Eng. Syst. Saf. 93 (2008) 364–372. doi:10.1016/j.ress.2006.12.010.
[29] A. V. Saetta, R. V. Scotta, R. V. Vitaliani, Analysis of chloride diffusion into partially saturated concrete, ACI Mater. J. 90 (1993) 441–451. doi:10.14359/3874.
[30] A. Ababneh, F. Benboudjema, Y. Xi, Chloride Penetration in Nonsaturated Concrete,

J. Mater. Civ. Eng. 15 (2003) 183–191. doi:10.1061/(ASCE)0899-1561(2003)15:2(183).

[31] T. Luping, L.O. Nilsson, Chloride binding capacity and binding isotherms of OPC pastes and mortars, Cem. Concr. Res. 23 (1993) 247–253. doi:10.1016/0008-8846(93)90089-R.

[32] E. Samson, J. Marchand, K.A. Snyder, J.J. Beaudoin, Modeling ion and fluid transport in unsaturated cement systems in isothermal conditions, Cem. Concr. Res. 35 (2005) 141–153. doi:10.1016/j.cemconres.2004.07.016.

[33] S.J.H. Meijers, J.M.J.M. Bijen, R. De Borst, A.L.A. Fraaij, Computational results of a model for chloride ingress in concrete including convection, drying-wetting cycles and carbonation, Mater. Struct. Constr. 38 (2005) 145–154. doi:10.1617/14133.

[34] Q.Z. Zhang, X.L. Gu, Z.L. Jiang, W.P. Zhang, Similarities in accelerated chloride ion transport tests for concrete in tidal zones, ACI Mater. J. 115 (2018) 499–507. doi:10.14359/51702007.

[35] Z.P. Bažant, L.J. Najjar, Nonlinear water diffusion in nonsaturated concrete, Matériaux Constr. 5 (1972) 3–20. doi:10.1007/BF02479073.

[36] A. V Saetta, B.A. Schrefler, R. V Vitaliani, The carbonation of concrete and the mechanism of moisture, heat and carbon dioxide flow through porous materials, Cem. Concr. Res. 23 (1993) 761–772.

[37] Y.P. Xi, Z.P. Bažant, H.M. Jennings, Moisture diffusion in cementitious materials Adsorption isotherms, Adv. Cem. Based Mater. 1 (1994) 248–257. doi:10.1136/adc.2007.131342.

[38] T. Ishida, T. Kishi, K. Maekawa, Multi-scale modeling of structural concrete, Crc Press, 2014.

[39] Z.L. Jiang, Y.P. Xi, X.L. Gu, Q.H. Huang, W.P. Zhang, Modelling of water vapour sorption hysteresis of cement-based materials based on pore size distribution, Cem. Concr. Res. 115 (2019) 8–19. doi:10.1016/j.cemconres.2018.09.015.

[40] W.P. Zhang, F. Tong, X.L. Gu, Y.P. Xi, Study on moisture transport in concrete in atmospheric environment, Comput. Concr. 16 (2015) 775–793. doi:10.12989/cac.2015.16.5.775.

[41] G. Lin, Y. Liu, Z. Xiang, Numerical modeling for predicting service life of reinforced concrete structures exposed to chloride environments, Cem. Concr. Compos. 32 (2010) 571–579. doi:10.1016/j.cemconcomp.2010.07.012.

[42] H.G. Min, W.P. Zhang, X.L. Gu, Effects of load damage on moisture transport and relative humidity response in concrete, Constr. Build. Mater. 169 (2018) 59–68. doi:10.1016/j.conbuildmat.2018.02.203.

[43] D. V. Val, R.E. Melchers, Reliability of Deteriorating RC Slab Bridges, J. Struct. Eng. 123 (1997) 1638–1644. doi:10.1061/(ASCE)0733-9445(1997)123:12(1638).

[44] M.G. Stewart, Q. Suo, Extent of spatially variable corrosion damage as an indicator of strength and time-dependent reliability of RC beams, Eng. Struct. 31 (2009) 198–207. doi:10.1016/j.engstruct.2008.08.011.

[45] M.S. Darmawan, Pitting corrosion model for reinforced concrete structures in a

chloride environment, Mag. Concr. Res. 62 (2010) 91–101. doi:10.1680/macr.2008.62.2.91.

[46] W.P. Zhang, B.B. Zhou, X.L. Gu, H.C. Dai, Probability distribution model for cross-sectional area of corroded reinforcing steel bars, J. Mater. Civ. Eng. 26 (2014) 822–832. doi:10.1061/(ASCE)MT.1943-5533.0000888.

[47] M. GB50068, Unified standard for reliability design of building structures, Minist. Hous. Urban-Rural Constr. People's Repub. China, Haidian Dist. Beijing, China. (2001).

Table list

Figure list

Fig. 15. Comparison of the mean of radius loss Δr and $\Delta r_{\max}$ under different ΔT_{50}

Fig. 16. PMF of repair combinations, e.g., 'CP2018 CPre2034' denotes the CP was activated at 2018 and CPre was activated at 2034

Fig. 17. CCDF of lifetime decision information

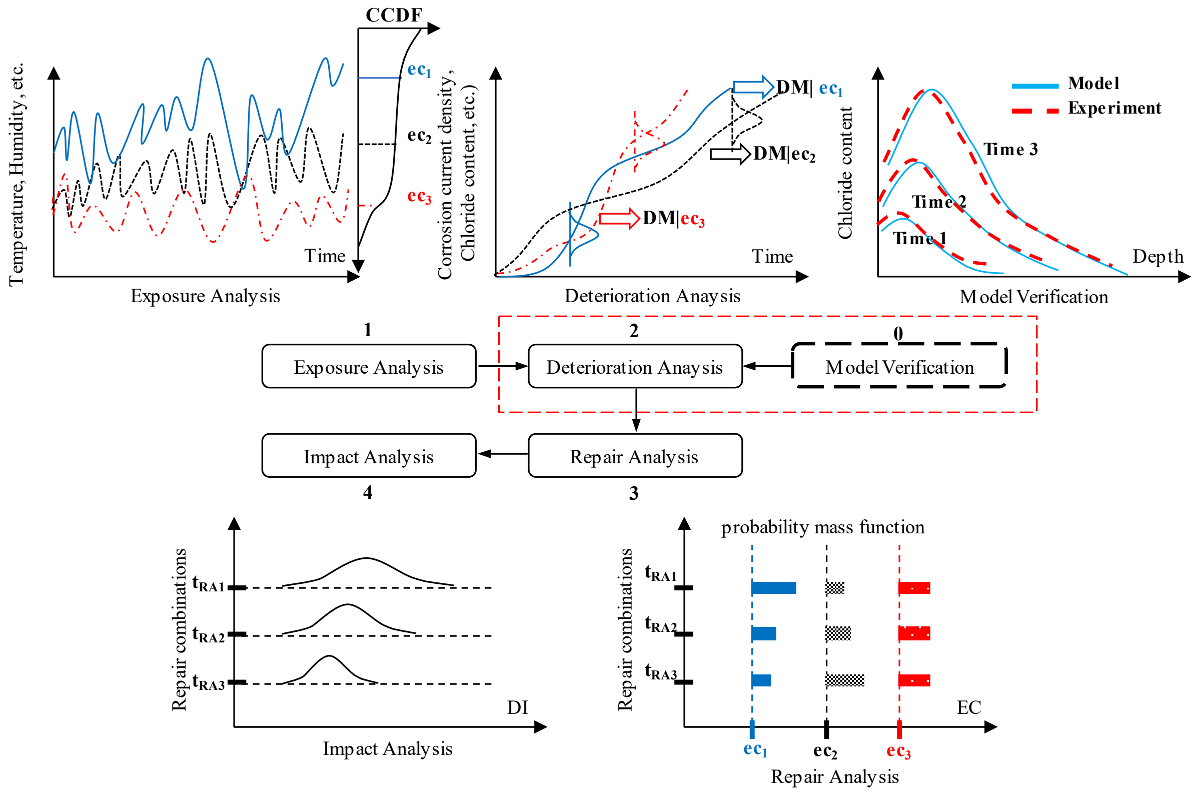

Fig. 1. Computational flowchart of the PBDE

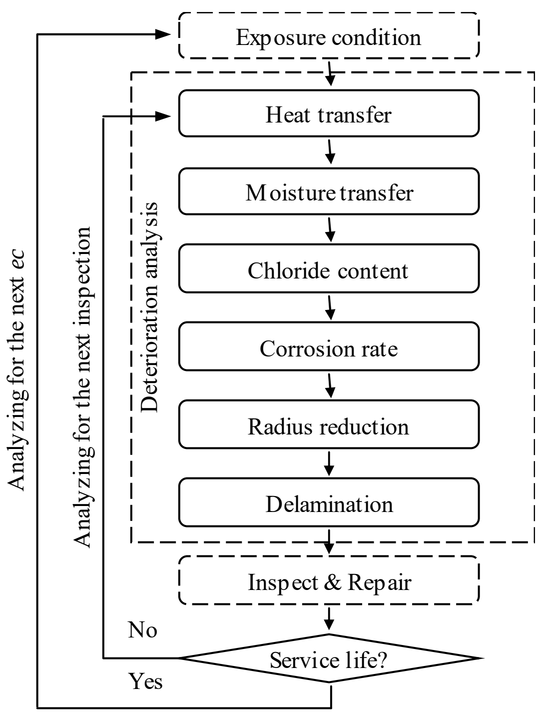

Fig. 2. Flowchart of the deterioration analysis

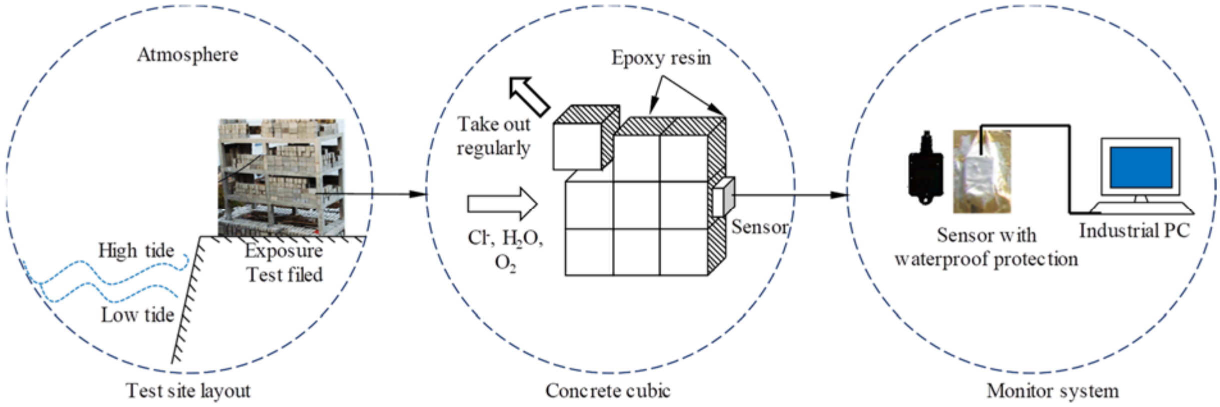

Fig. 3. Illustrative figures of the exposure test

Note: Photos come from Ref. [17]

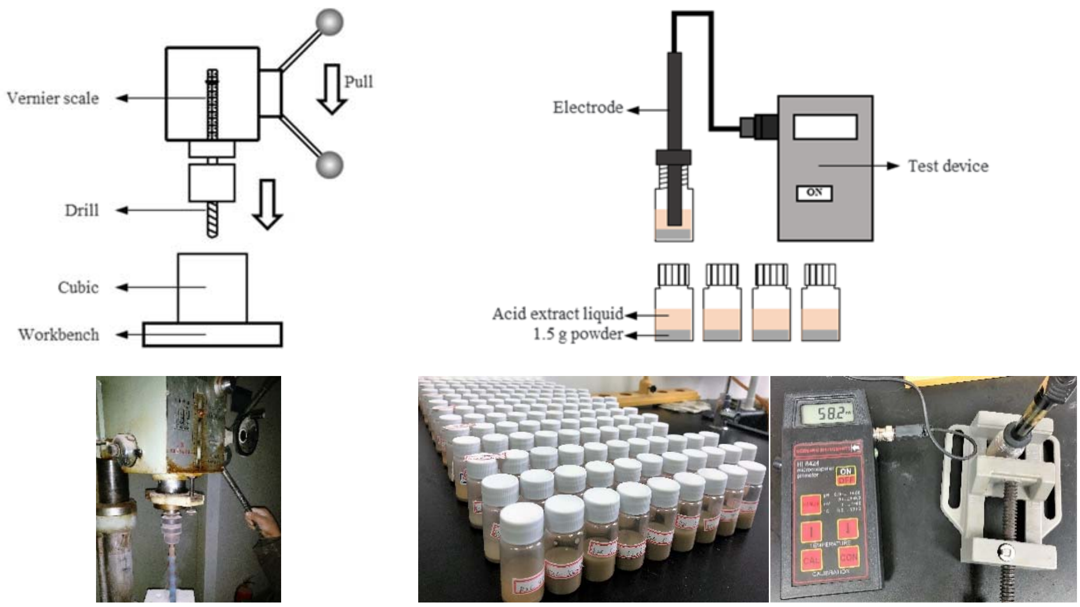

(a) Powder drilling

(b) Test of Chloride concentration

Fig. 4. Illustration of chloride concentration measurement

Note: Photos were shot by the first author

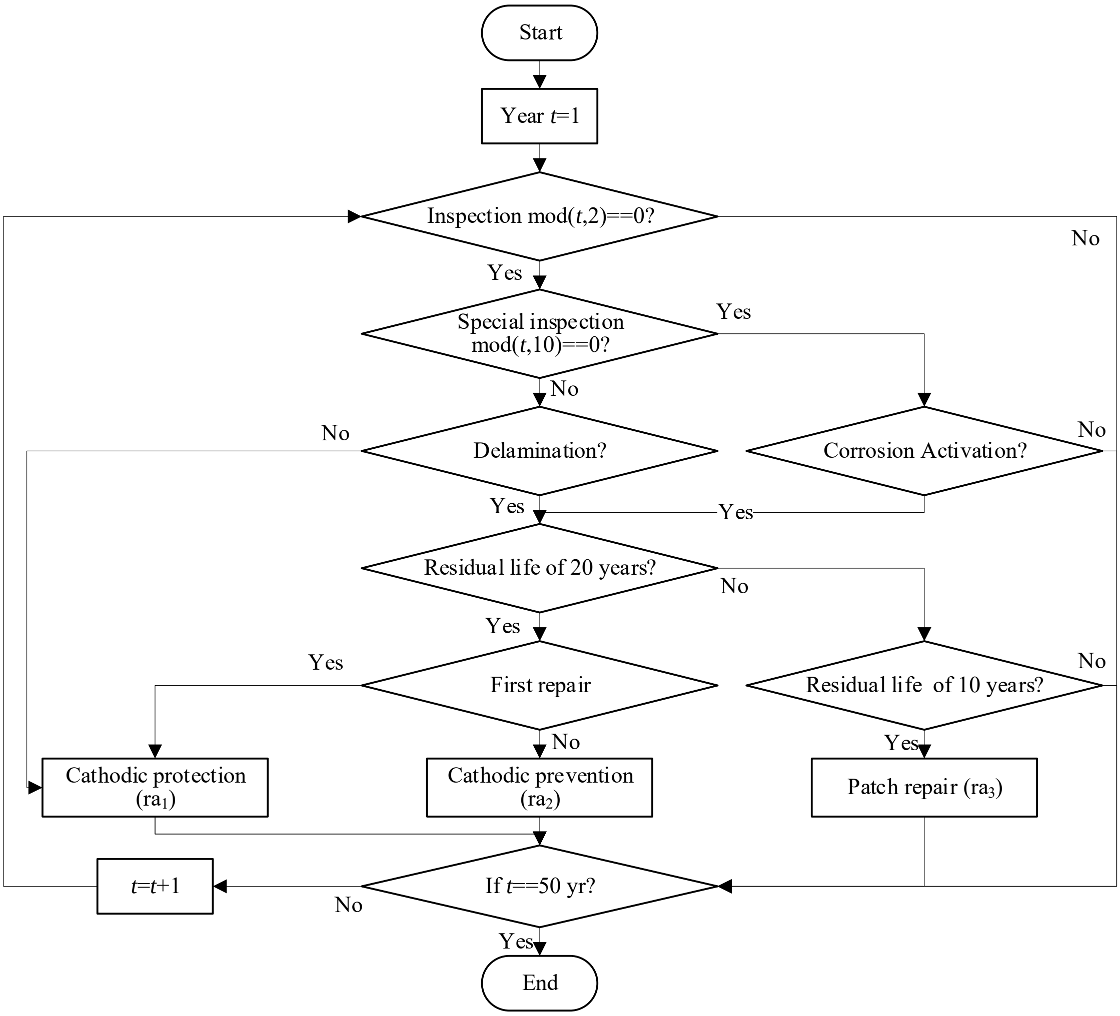

Fig. 5. Decision tree model of repair actions within the service life

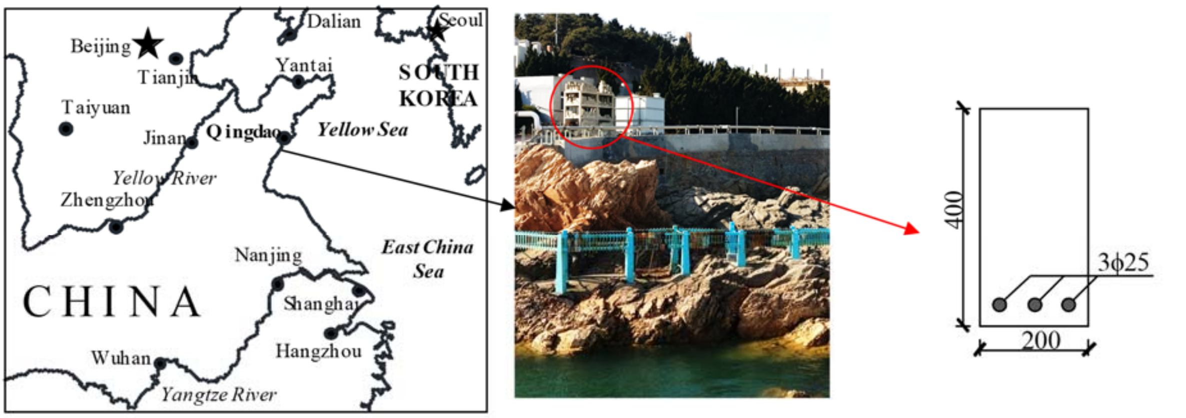

(a) Location on the map (b) Exposure site (c) Cross-section of RC beam

Fig. 6. Investigated corroded RC beam

Note: Photo was shot by the first author

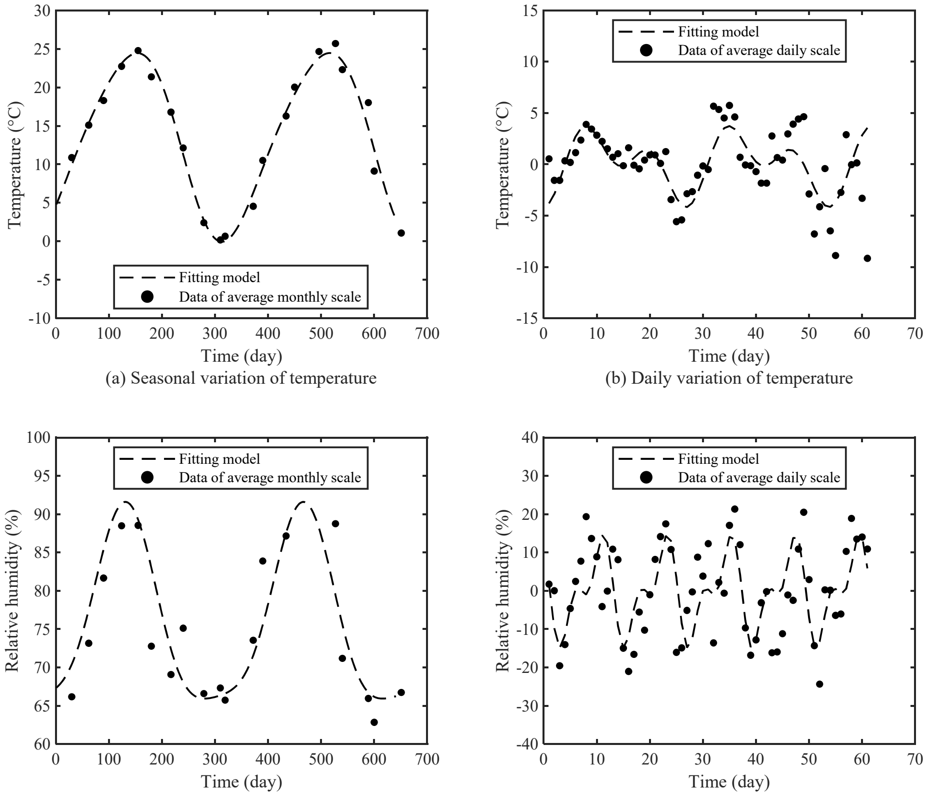

(a) Seasonal variation of temperature (b) Daily variation of temperature

(c) Seasonal variation of humidity (d) Daily variation of humidity

Fig. 7. Comparisons between the numerical model and measured data of temperature and relative humidity

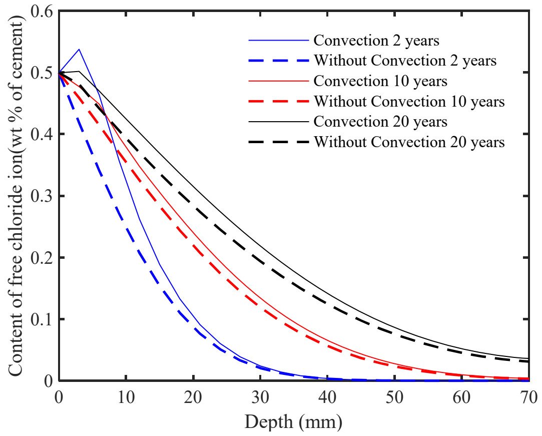

Fig. 8. Comparison of free chloride profiles within concrete under the assumptions of with and without convection

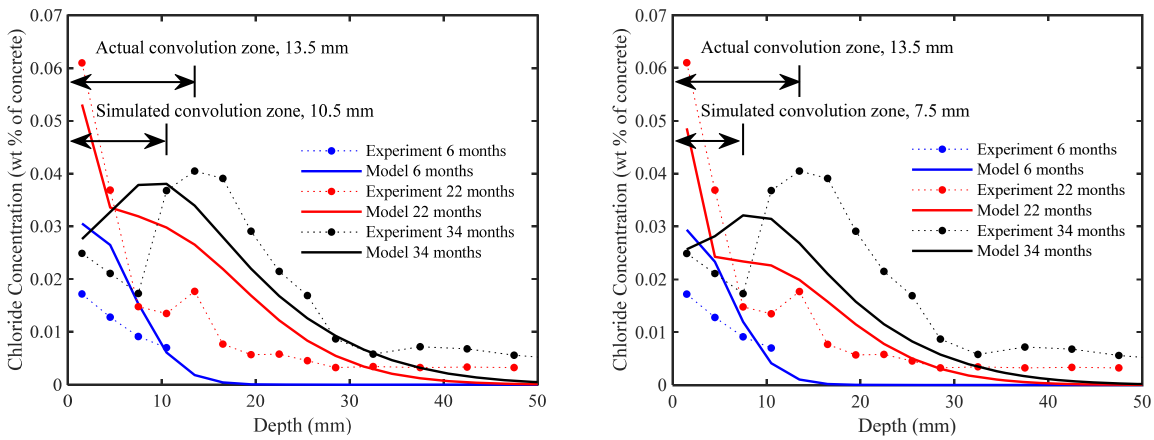

(a) With convection (b) Without convection

Fig. 9. Comparison between the prediction model and experimental data of chloride transport within concrete

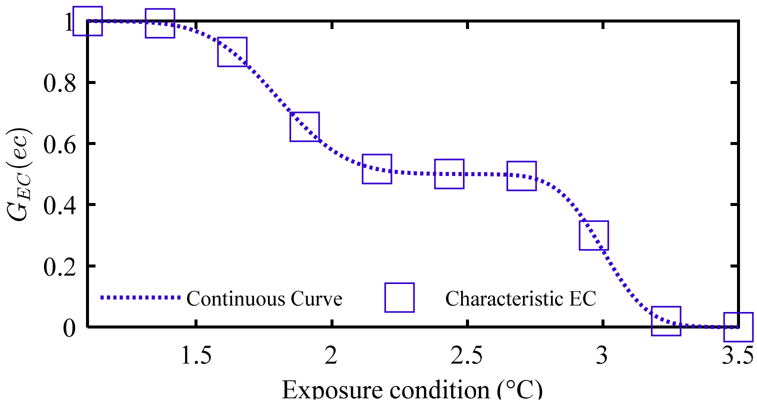

Fig.10. Discretized CCDF of exposure condition

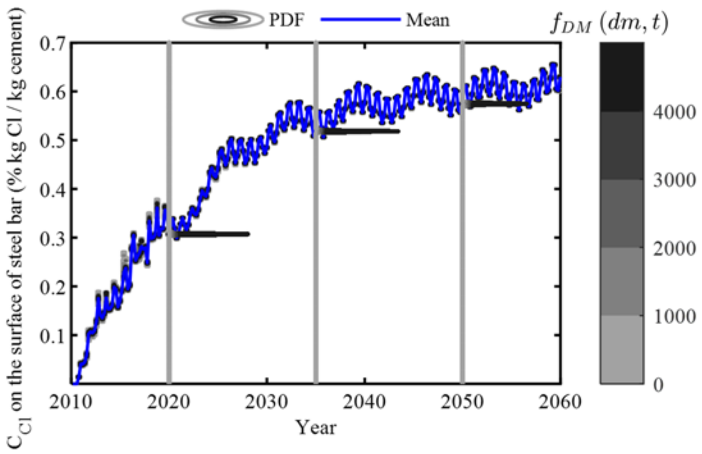

(a) Evolution of chloride content on the surface of the corner reinforcement of Case 1

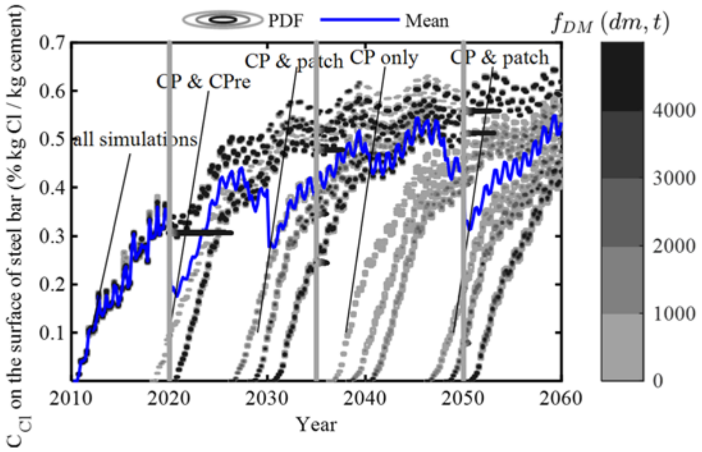

(b) Evolution of chloride content on the surface of the corner reinforcement of Case 5

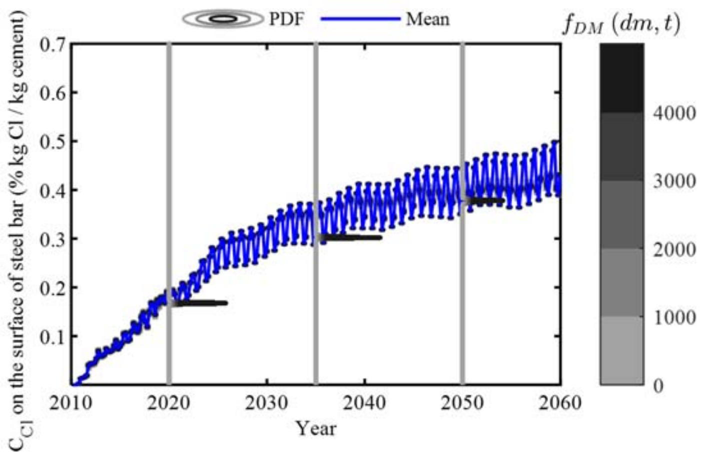

(c) Evolution of chloride content on the surface of the middle reinforcement of Case 1

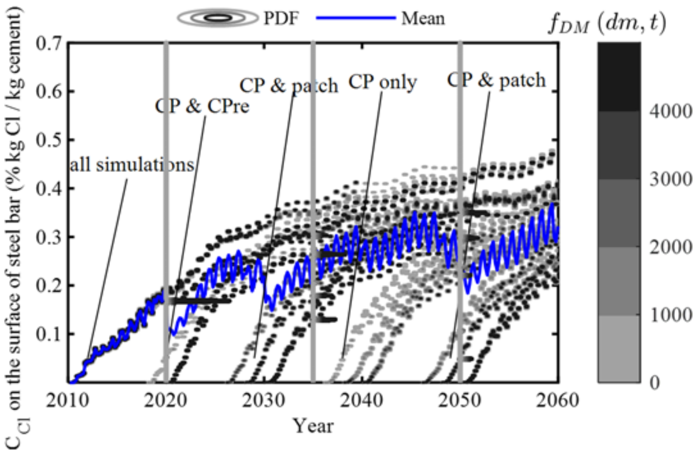

(d) Evolution of chloride content on the surface of the middle reinforcement of Case 5

Fig. 11. Contour plots of PDF surface of chloride concentration on the steel bar surface in the Case 1 and Case 5 (Contours are plotted at f_{dm}= $\{0,10^3, 2\times10^3, 3\times10^3, 4\times10^3\}$ and PDF are drawn horizontally by 1/5000 scale against vertical axes at 2020, 2035 and 2050)

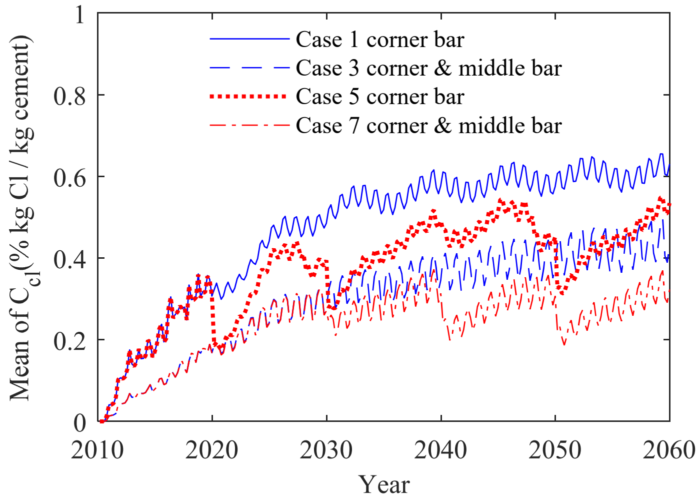

(a)

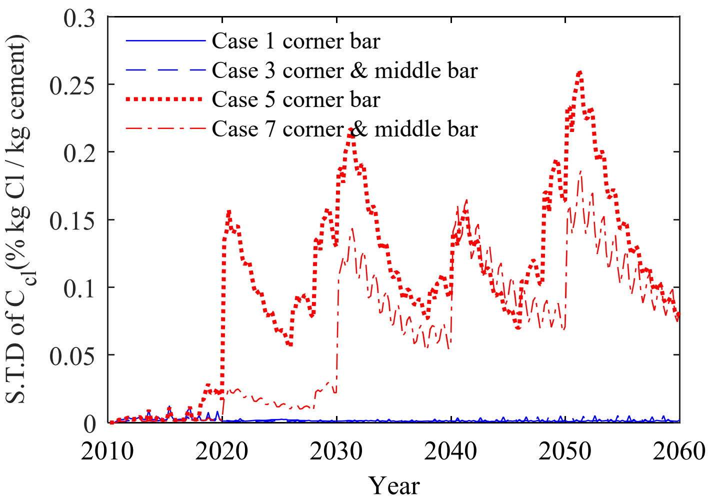

(b)

Fig.12. Comparison of the mean and STD of chloride concentration on the steel bar surface (Note: 'Case 1 corner/middle bar' denotes the results of surface the corner/middle steel bar under Case 1)

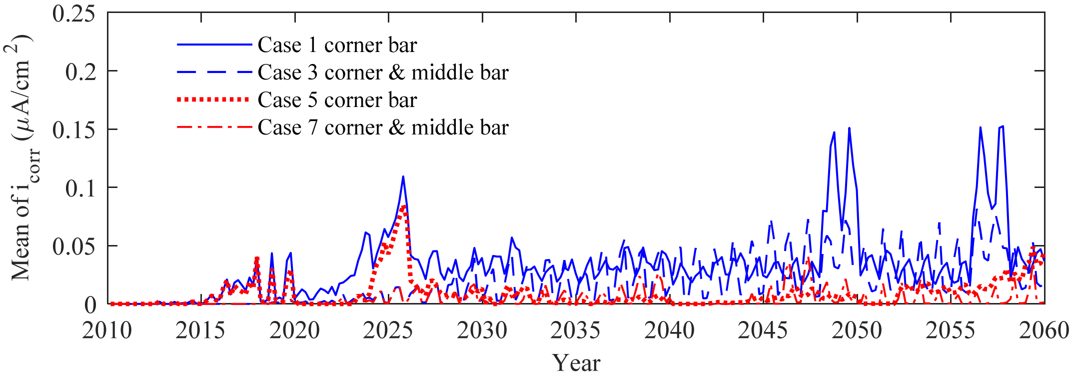

(a)

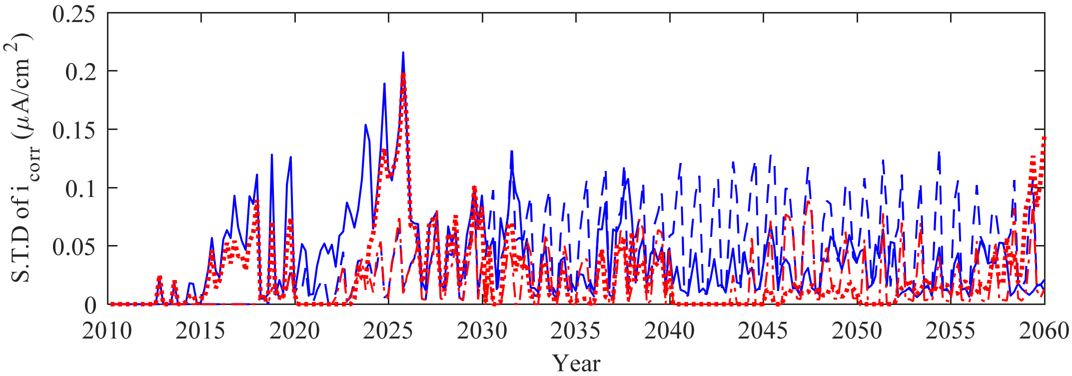

(b)

Fig. 13. Comparison of the mean and STD of corrosion current density

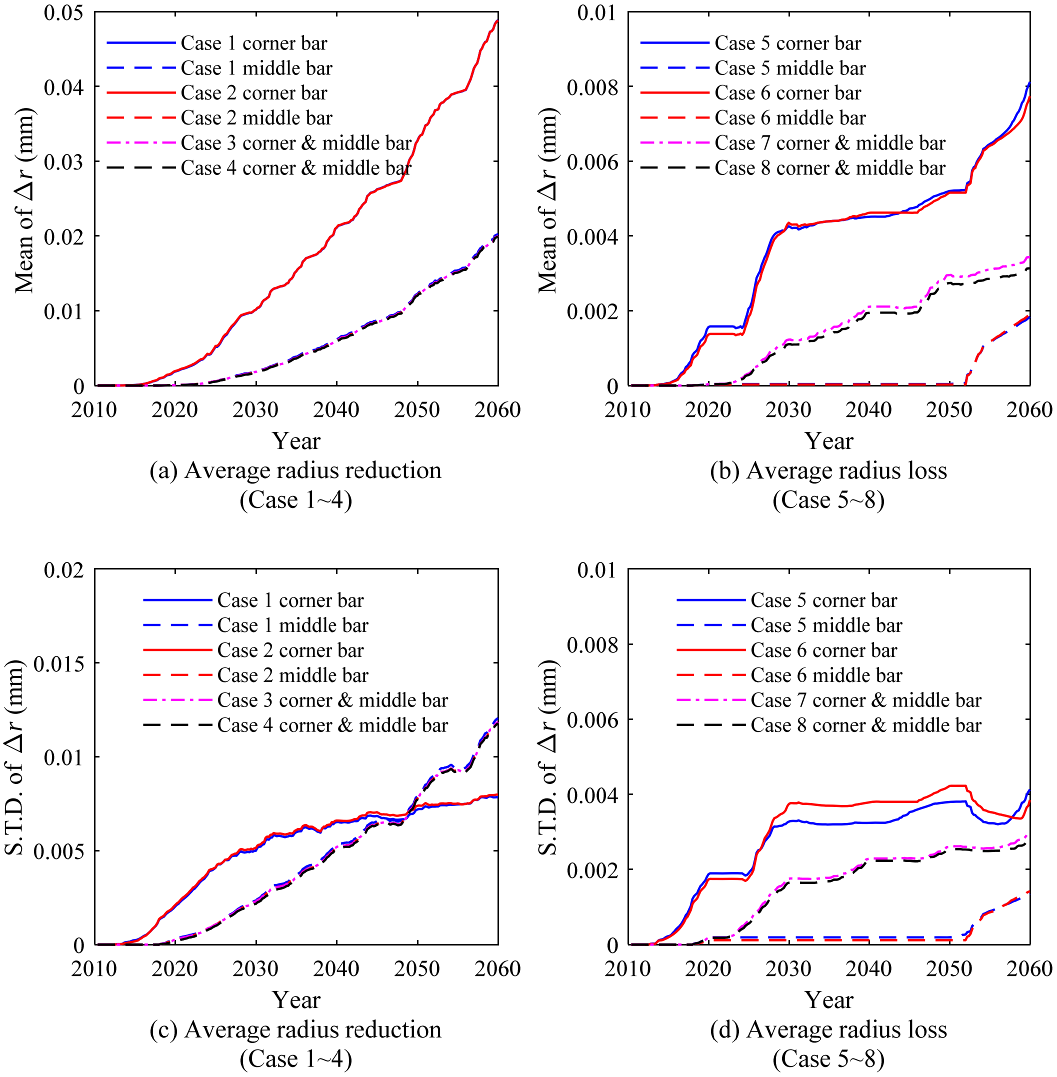

(a) Average radius reduction (Case 1~4)

(b) Average radius loss (Case 5~8)

(c) Average radius reduction (Case 1~4)

(d) Average radius loss (Case 5~8)

Fig. 14. Comparison of the mean and STD of the average loss of reinforcement radius Δr under Cases 1~8

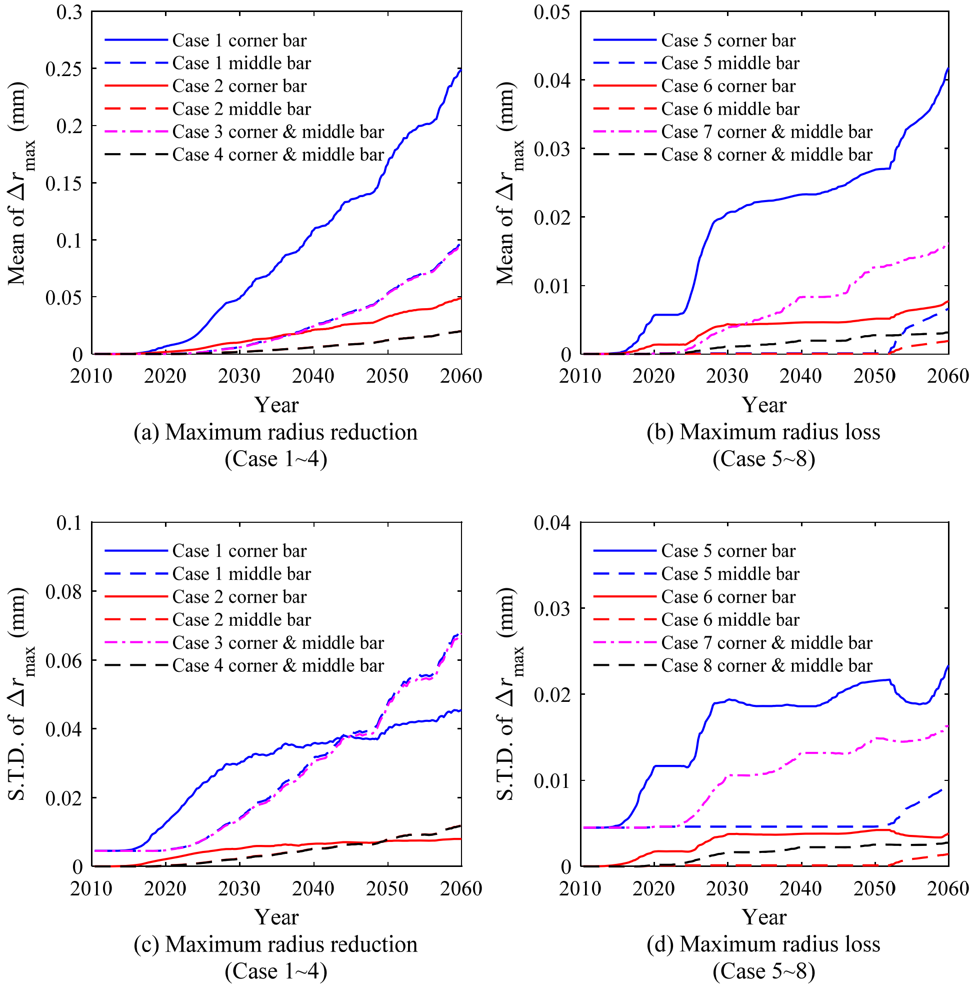

(a) Maximum radius reduction (Case 1~4)

(b) Maximum radius loss (Case 5~8)

(c) Maximum radius reduction (Case 1~4)

(d) Maximum radius loss (Case 5~8)

Fig. 15. Comparison of the mean and STD of maximum loss of reinforcement radius Δr_{max} under Case 1~8

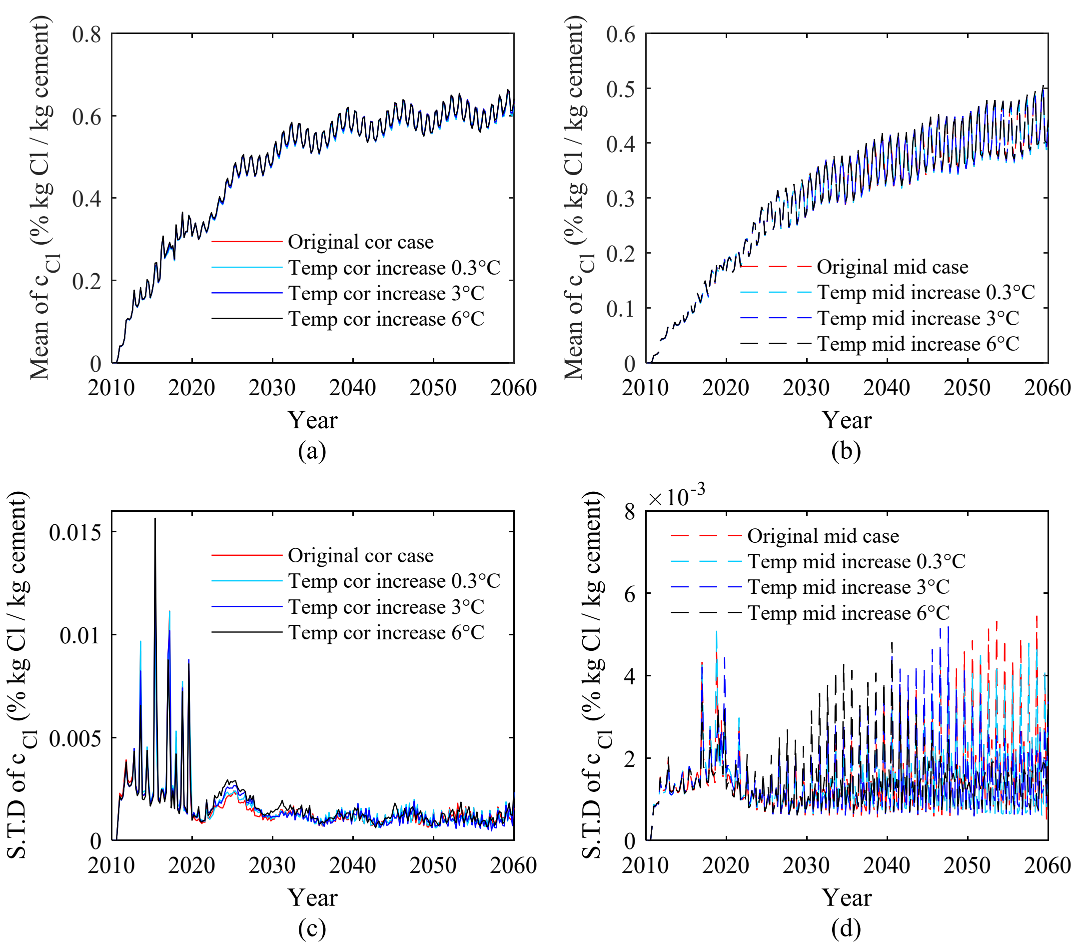

Fig. 16. Comparison of the mean and STD of chloride concentration on the steel bar surface under different ΔT_{50}

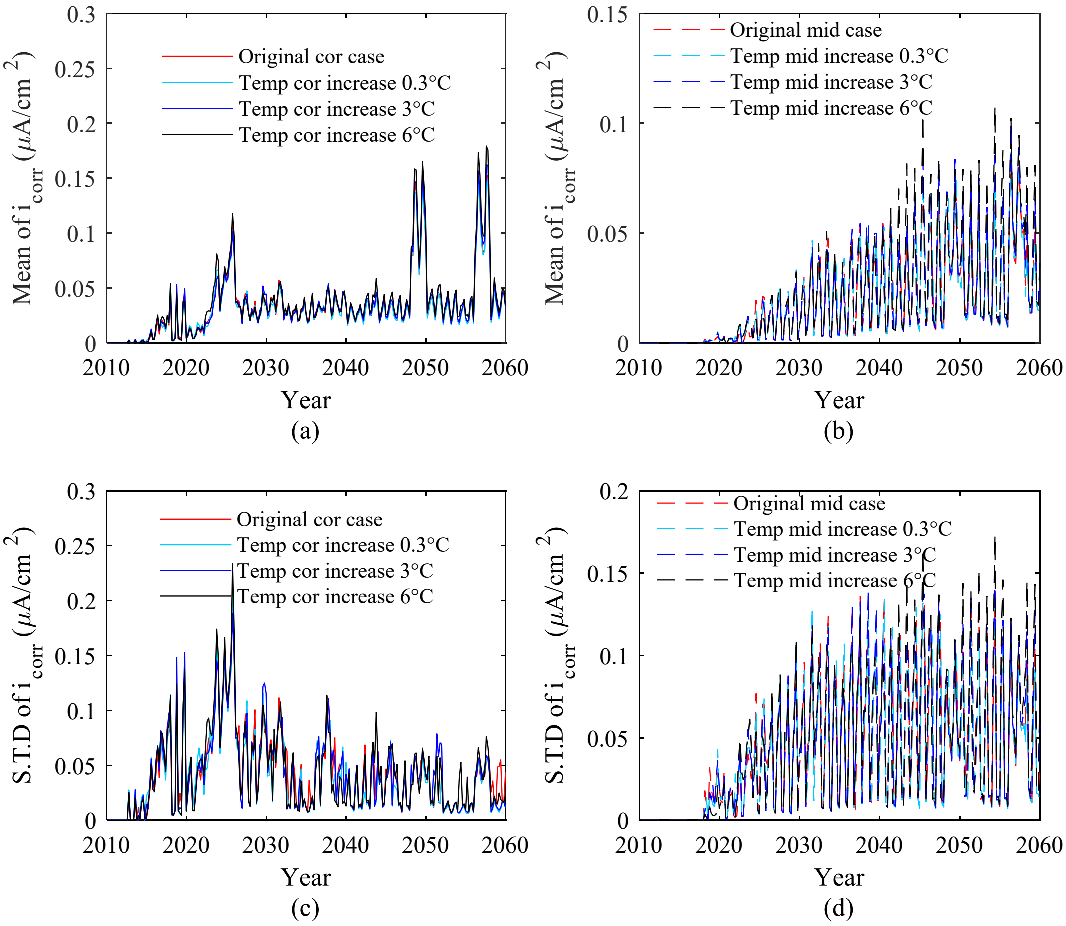

Fig. 17. Comparison of the mean and STD of corrosion current density under different ΔT_{50}

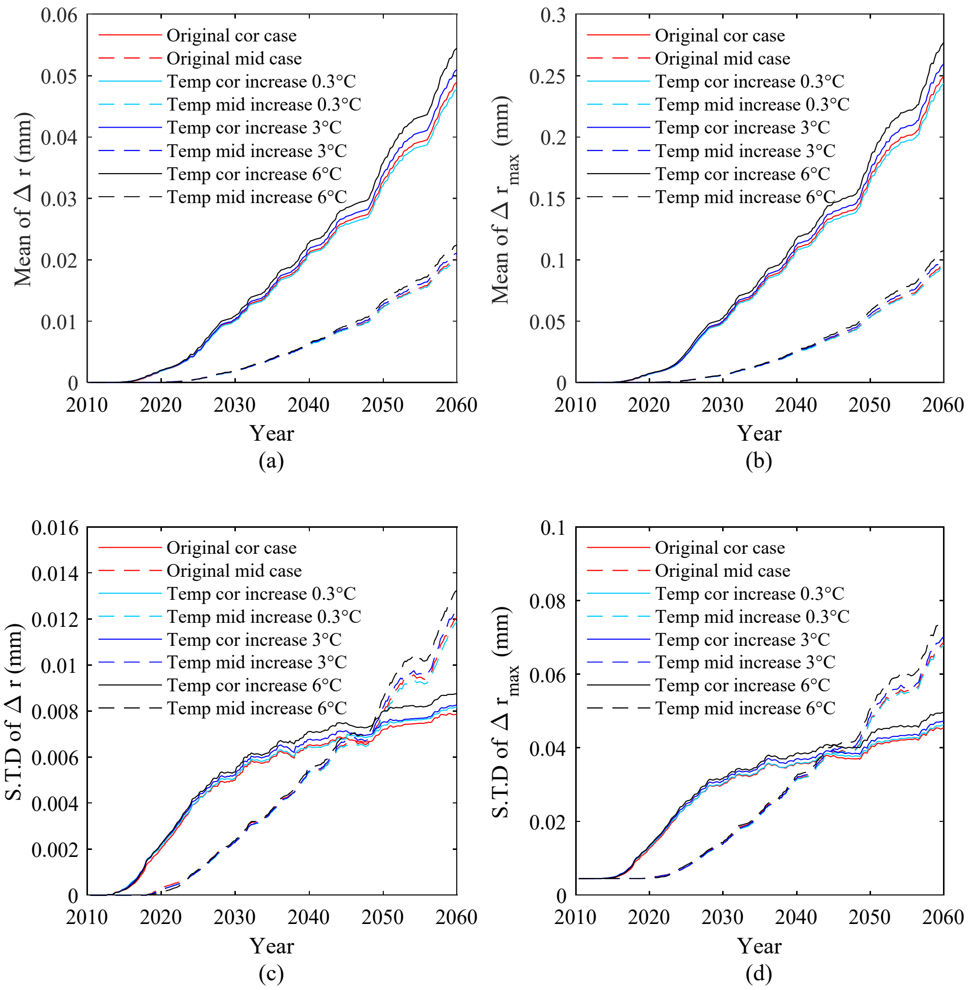

Fig. 18. Comparison of the mean and STD of radius loss Δr and $\Delta r_{\max}$ under different ΔT_{50}

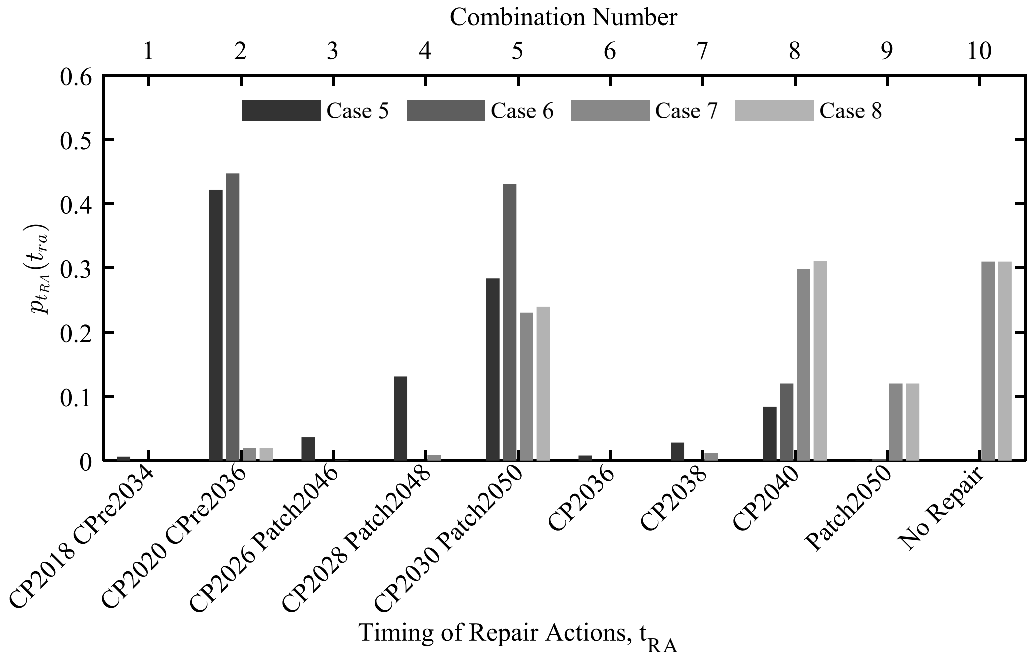

Fig.19. PMF of repair combinations, e.g., 'CP2018 CPre2034' denotes the CP was activated at 2018 and CPre was activated at 2034

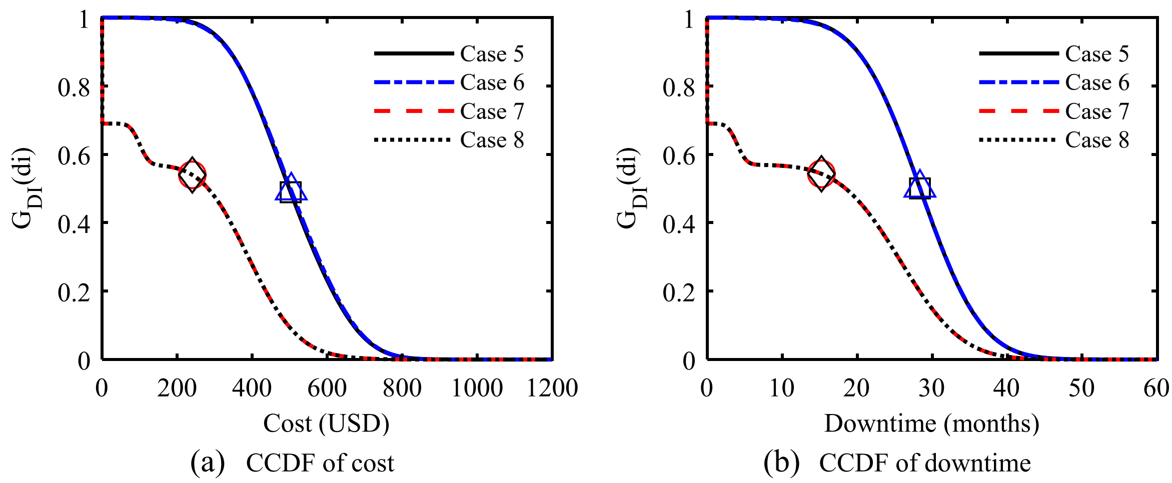

Fig. 20. CCDF of lifetime decision information

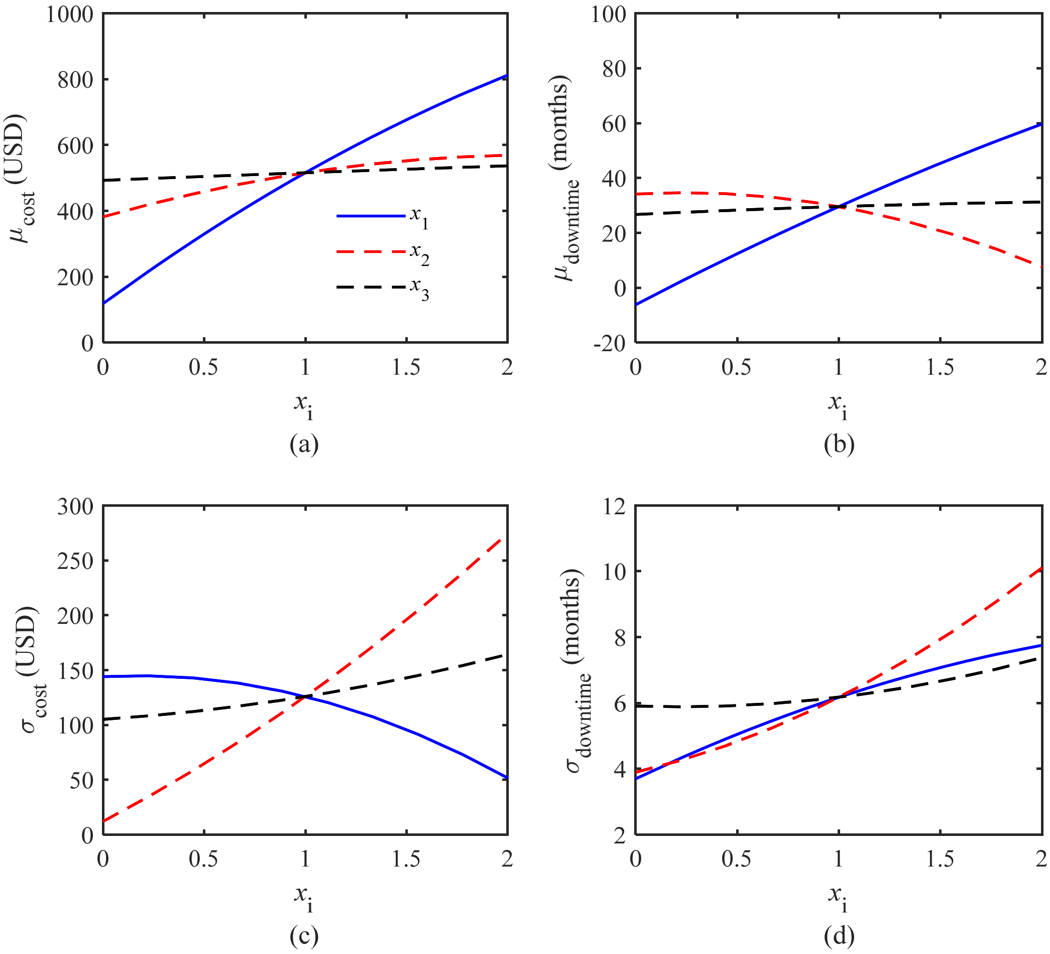

Fig. 21. Relationship between x_i and the distribution parameters of decision information under Case 5

Table 1. Investigated eight cases

	Case 1	Case 2	Case 3	Case 4	Case 5	Case 6	Case 7	Case 8
Repair action	Unapplied	Unapplied	Unapplied	Unapplied	Applied	Applied	Applied	Applied
Chloride transport	2D	2D	1D	1D	2D	2D	1D	1D
Non-uniform corrosion	Yes	No	Yes	No	Yes	No	Yes	No

Table 2. Related parameters and values

Parameter name	Value	Recourse
$D_{\mathrm{c,ref}}$ ($\mathrm{m^2/s}$)	6×10^{-12}	[17]
$D^{dry}_{\mathrm{h,ref}}$ ($\mathrm{m^2/s}$)	3×10^{-10}	[42]
$D^{wet}_{\mathrm{h,ref}}$ ($\mathrm{m^2/s}$)	15×10^{-10}	[42]
T_{ref} (K)	296	[28]
t_{ref} (d)	28	[28]
h_c	0.75	[37]
m	0.15	[37]
n	11	[37]
α_0	0.05	[37]
R_{gas} ($\mathrm{Jmol^{-1}K^{-1}}$)	8.314	[28]
ρ_{c} ($\mathrm{kg/m^3}$)	2401	[17]

Table 3. Parameters used in the environmental model

Parameters	Temperature	Humidity	Surface chloride content
a_1	-12.02	0.13	0.052
a_2	1.35	-0.03	-
ec	1.10	-	-
a_{ec}	0.0317	-	-
b_1	2.27	5.43	-0.056
b_2	-5.39	-0.29	-
n_{ec}	0.7279	-	-
bam	12.78	0.76	0.099
w_1	6.33	6.84	-
t_{ref} (day)	149	149	-
a_{01}	0.1326	-0.0942	-
a_{11}	2.111	5.866	-
b_{11}	1.012	-8.576	-
w_{11}	0.2333	0.5206	-
a_{21}	2.188	6.334	-
b_{21}	0.3616	-2.548	-

Table 4. The ratio of mean and STD of C_{Cl}, i_{corr}, Δr and Δr_{max} under different scenarios to Case 1

Bar Type	Data Type	ΔT_{50}	C_{Cl}	i_{corr}	Δr	Δr_{max}
Corner bar	Mean	0.3	0.995	0.883	0.977	0.978
		3	1.006	0.889	1.042	1.042
		6	1.017	0.913	1.114	1.111
	STD	0.3	1.490	0.256	1.042	1.018
		3	1.484	0.256	1.055	1.042
		6	1.650	0.529	1.115	1.093
Middle bar	Mean	0.3	0.998	0.918	0.976	0.978
		3	1.012	1.491	1.040	1.044
		6	1.030	2.117	1.105	1.114
	STD	0.3	1.224	0.376	0.984	0.989
		3	1.301	1.771	1.024	1.022
		6	1.375	2.483	1.098	1.092

Table 5. β_k (k = 0,1,…,9) coefficient within RSM function

	μ_{cost} (USD)	$\mu_{downtime}$ (Months)	σ_{cost} (USD)	$\sigma_{downtime}$ (Months)
β_0	-74.31	-7.31	29.04	1.76
β_1	455.29	40.67	33.01	3.20
β_2	207.07	6.40	49.10	0.28
β_3	55.24	4.73	-3.01	-0.53
β_4	-50.42	-2.82	-28.08	-0.45
β_5	-4.48	-1.58	4.60	0.29
β_6	-2.88	-0.50	-27.62	-0.56
β_7	-40.40	-8.69	17.43	0.83
β_8	-28.30	-0.69	42.65	0.88
β_9	-0.99	-0.63	8.78	0.47